

From Street View to Visibility Network: Mapping Urban Visual Relationships with Vision–Language Models

Zicheng Fan^a, Kunihiko Fujiwara^{a,b}, Pengyuan Liu^c, Fan Zhang^d, Filip Biljecki^{a,e,*}

^a*Department of Architecture, National University of Singapore, Singapore*

^b*Research & Development Institute, Takenaka Corporation, Japan*

^c*Urban Analytics Subject Group, Urban Studies & Social Policy Division, University of Glasgow, United Kingdom*

^d*Institute of Remote Sensing and GIS, Peking University, China*

^e*Department of Real Estate, National University of Singapore, Singapore*

Abstract

Visibility analysis in urban planning has traditionally relied on line-of-sight (LoS) simulations, which capture geometric occlusion. But these require accurate 3D data that is seldom available and often fail to represent how specific urban objects (e.g., landmarks) are visually encountered in real streetscapes. We reformulate object visibility assessment as an urban visual search problem in image space and take advantage of the omnipresent availability of street view imagery (SVI): given a reference image of the target object, we search for where it is visually detectable in SVI, bypassing the need for 3D or high-resolution elevation models. Specifically, a Vision Language Model (VLM) is applied to detect the target object within direction and zoom-controlled SVI. Successful detection represents the object’s visibility at the corresponding viewpoint. Further, taking traditional visibility analysis forward, a heterogeneous visibility graph is constructed to model the interaction between viewpoints and target objects. This graph enables mapping where visual connections occur, how strong they are, and how multiple landmarks become jointly connected through shared viewpoints. In a case study across six tall landmark constructions in global cities, the image-based method achieves an overall accuracy of 87% and reveals contextual differences in how landmarks are perceived and experienced in surrounding urban fabrics.

*Corresponding author.

In another case along the River Thames in London, the visibility graph uncovers the form and strength of multi-landmark connections and pinpoints the locations that mediate them. Bridges account for approximately 30% of all connections. Our method can serve as an effective alternative to traditional LoS-based visibility analysis, and showcases the possibility of revealing the prevalent connection of a wide range of visual objects in the urban environment. It opens up new research perspectives for urban planning, heritage conservation, and computational social science.

Keywords:

Urban Landmarks, Line of Sight, Visibility, Vision-language Model, Heterogeneous Graph

1. Introduction

Visibility analysis is a fundamental analytical method in urban and environmental research, and is primarily conducted based on the Line of Sight (LoS) principle (Fisher-Gewirtzman et al., 2013; Cilliers et al., 2023). LoS establishes a hypothetical direct line between an observer and the target object, with the presence of an uninterrupted line indicating visibility. Owing to its simplicity and intuitive nature, LoS has been widely adopted and underpins more advanced visibility analyses, such as viewshed analysis (Tandy, 1967; Amidon and Elsner, 1968), isovist analysis (Benedikt, 1979; Batty, 2001), to map the extent and boundaries of visible space, and visibility graph analysis to investigate the spatial relationship defined by visual links (Turner et al., 2001).

Despite the widespread use, visibility analysis based on LoS faces two key limitations when applied in the 3D urban environment: First, its reliability relies on the completeness and resolution of the underlying spatial data models, such as building footprints with associated height attributes, 3D city models, Digital Surface Models (DSM), and Digital Elevation Models (DEM) (Wróżyński et al., 2024; Cilliers et al., 2023; Morello and Ratti, 2009; Lei et al., 2023). High-quality and open 3D datasets are still scarce in many cities, and studies continue to rely on 10–30 m DEMs, a resolution that can misrepresent LoS and introduce substantial error (Inglis et al., 2022). At the same time, there are other urban data sources such as Street View Imagery (SVI) that are almost ubiquitous, but have not been used for such use case. Thus, it is worthwhile to investigate whether there are other urban data sources that could be used in lieu of 3D data, allowing visibility analyses to be conducted where there is no 3D data available.

Second, traditional LoS-based methods can be blind to visual context and inter-object relationships, aspects central to human perception (Gillings and Wheatley, 2001; Déderix, 2019; Inglis et al., 2022). By treating visibility as a mere geometric intersection, they overlook the environmental context, such as lighting, vegetation, advertising boards, architectural embellishments, and the way multiple objects share a view. The challenge becomes evident when analysing named objects such as urban landmarks. Tracing an unobstructed LoS to the apex of a landmark may confirm it is “visible,” but this says little about how the landmark is framed by neighbouring buildings, how much of its recognisable silhouette emerges beyond tree canopies, or how it co-occurs with other icons along a skyline or view corridor. In which ways landmarks are perceived in urban environment are especially emphasised in spatial planning and heritage conservation fields (Lopes et al., 2019; Czyńska and Rubinowicz, 2019; Ashrafi et al., 2021; Talamini et al., 2023). However, without incorporating the contextual cues and inter-object relationships, LoS analysis cannot capture the perceptual reality that planners, designers, and everyday observers actually experience.

Unlike LoS analysis, which simulates the visual process based on data models, images record the outcome of visibility in place, capturing real-world visual relationships directly. In previous practices, images often serve as supplementary reference to LoS-based visibility analysis, offering intuitive insights about both visibility and visual contexts (Greater London Authority, 2012; Talamini et al., 2023). While their potential for large-scale, high-quality visibility assessments of urban objects remains underexplored. Two recent advancements offer opportunities for quantitatively detecting LoS from images. First, the emergence of Vision-Language Models (VLM), such as CLIP (Radford et al., 2021), OWL-ViT (Minderer et al., 2022, 2024), Grounding DINO (Liu et al., 2024) have significantly lowered the barrier to extracting semantic information and open-domain objects from images. These advancements enable identifying named urban objects with distinct visual characteristics, such as unique height, architectural style, or shape. Second, the potential of SVI as an important geo-located data source is receiving more attention in urban and geographical studies (Ito et al., 2024). SVI is typically used to observe and map the foreground space of a city for less visual obstruction (Fan et al., 2025), while neglecting distant objects in the background. However, as shown in Figure 1, certain iconic urban landmarks (e.g., The Shard in London) can be occasionally observed from SVI at street level, from varying distances and urban settings. Furthermore, because SVI is widely available across urban streets, it forms a dense and interconnected set of geo-referenced view-points, allowing visibility analysis to move beyond isolated locations toward a

city-scale visibility network.

Given the gaps and opportunities, this study explores an image-based visibility detection method that leverages computer vision and geo-located SVI, offering a data-driven alternative to conventional LoS-based visibility analysis. The questions to answer in this study include:

1. Can images be quantitatively applied as a scalable alternative to 3D models, to investigate the visibility of urban objects?
2. Can image-based visibility analysis provide valuable insights into the visual and spatial context of observations?
3. To what extent can images reveal the visual relationships among multiple objects and their interaction with the urban environment?

A research framework is presented in Figure 1. Firstly, we introduce the workflow to detect the visibility of distant urban objects via SVI. Using a case study, we assess the method’s reliability in evaluating the visibility of the iconic high-rise landmarks across global cities. We also prove its unique value in revealing the visual context of observation compared to other methods. We then extend the application of image-based visibility to analysing inherent visual relationships among multiple urban objects by developing a novel heterogeneous visibility graph. Using the second case study, we examine the inter-visibility, visual co-existence and generalisable visual-spatial connection among multiple landmarks along the River Thames in London, UK. The advantages, limitations and practical applications of the proposed method are discussed accordingly.

2. Background and Related Work

2.1. Urban Landmarks and their Visual Significance

Urban landmarks are deeply tied to the identity and spirit of their cities and serve as recognisable visual symbols (Manahasa et al., 2024). In environmental perception research, the landmark is identified as one of the fundamental elements in the typology of interrelated urban forms (Lynch, 1996). There is a multi-facet impact of landmarks on spatial cognition and way-finding of human beings (Evans et al., 1982; Lee and Tversky, 2005; Epstein et al., 2017; Yesiltepe et al., 2021). Specifically, memory and recall of landmarks facilitate pedestrians’ identification of routes and scenes (Bruns and Chamberlain, 2019). By incorporating landmarks for consideration, Agent-Based Model (ABM) achieves better simulation of human navigation (Filomena and Versteegen, 2021). Furthermore, landmarks possess outstanding socio-economic value due to their attraction for tourism, commercial,

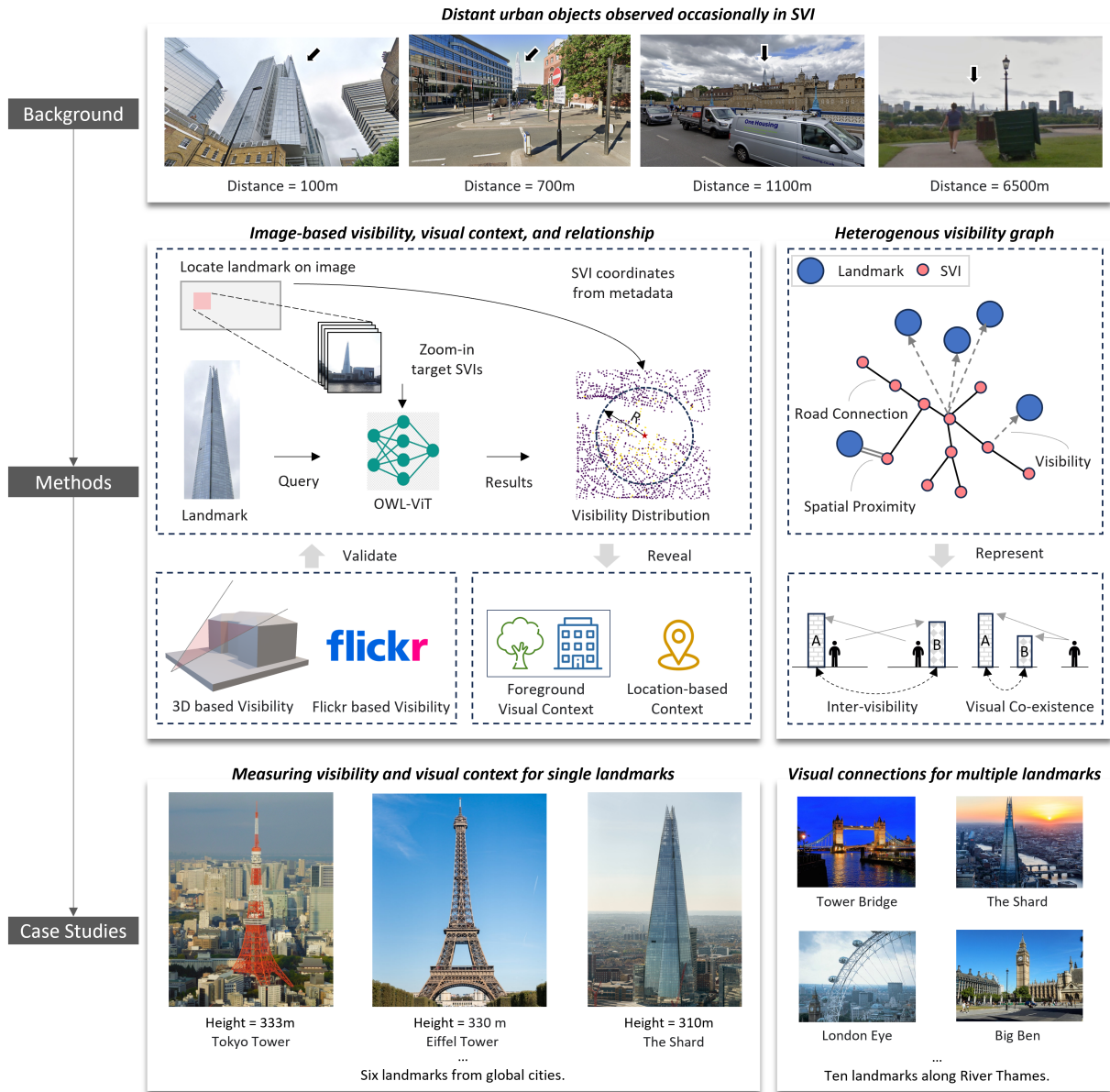


Figure 1: A research framework for the study. Imagery: Google Street View, Wikimedia Commons, Tripadvisor.

and cultural activities (Truchet et al., 2016). Access or view to landmarks also adds to the property value (Turan et al., 2021; Franco and Macdonald, 2018).

Due to their significance, urban authorities often aim to preserve long-established visual relationships with landmarks, such as visibility from designated viewpoints and directions (Tavernor, 2007). The visual quality, impact, and landscape components of landmarks are also emphasised, especially in spatial planning and heritage conservation fields (Czyńska and Rubinowicz, 2019; Ashrafi et al., 2021; Talamini et al., 2023). New developments are supposed to make positive contributions to the existing views. In practice, the London View Management Framework has established eight protected vistas of St. Paul's Cathedral, imposing height restrictions on buildings that might obstruct these landmarks (Greater London Authority, 2012). Similarly, the City of Vancouver implements the Public Views Guidelines to preserve the downtown skyline and maintain views towards its renowned mountainous and waterfront landscapes (City of Vancouver, 2024).

2.2. Common Methods and Limitations for Investigating Visibility

2.2.1. 2D and 3D Visibility Analysis

Visibility analysis, based on the Line of Sight (LoS) principle, is fundamental in urban planning and landscape research, and has been widely applied to investigate the visual condition and impact of urban landmarks (Santosa et al., 2023; Pyka et al., 2022; Mor et al., 2021; Czyńska and Rubinowicz, 2019; Bartie et al., 2015).

Historically, 2D visibility analysis emerged first and gained wide application in architectural and urban design fields. By assuming uniform ground elevation and treating environmental obstructions (e.g., walls, buildings, trees) as binary barriers, 2D LoS simplifies the definition and identification of visibility. This simplification enabled early exploration of visual relationships and spatial configurations. A classical method is isovist analysis, introduced by Tandy (1967) and refined by Benedikt (1979), which defines and describes the immediate visible area from a given observer location. Isovist-based 2D methods are widely used to evaluate building layouts (Batty, 2001; Hosseini Alamdari et al., 2022) and investigate human perception and behaviour in the space (Wiener and Franz, 2005; Krukar et al., 2021; Snopková et al., 2023). However, 2D methods often rely on oversimplified assumptions about ground uniformity and remove metric information (Ratti, 2004), constraining their applicability in complex terrains and vertical morphologies.

To overcome these constraints, 3D visibility analysis evolved to simulate real-world scenes more accurately. Several studies extended isovist analysis to 3D

spatial environments (Hagberg et al., 2008; Kim et al., 2019; Krukar et al., 2021). In parallel, 3D viewshed analysis has become common practice in large-scale applications such as evaluating landscape visual quality (Czyńska and Rubinowicz, 2019; Swietek and Zumwald, 2023) or assessing the visual impact of new developments (Inglis et al., 2022; Klouček et al., 2015; Alphan, 2021; Cilliers et al., 2023). 2.5D data models, such as the Digital Surface Models (DSM), Digital Elevation Models (DEM), and vector-based building data, are applied to simulate the real-world environment surfaces (Wróżyński et al., 2024). Viewshed, cumulative viewshed, and fuzzy viewshed analyses (Cilliers et al., 2023) are now standard tools in GIS platforms (e.g., ArcGIS (ESRI, 2021), QGIS (Cuckovic, 2016), GRASS (Neteler et al., 2012)). Despite their enhanced realism, 2.5D models frequently lack semantic differentiation and are restricted to representing complex 3D morphology (Pyka et al., 2022). To address this, recent studies apply true 3D data, such as LiDAR point clouds and voxel grids, to enhance detail and accuracy (Kim et al., 2019; Wu et al., 2021; Zhao et al., 2020; Wróżyński et al., 2024; Fujiwara et al., 2026). For instance, Czyńska and Rubinowicz (2019) employed a high-resolution (0.5 m grid) and semantically enriched DSM to quantify the exposure levels and spatial extent of five prominent landmarks in Lublin, Poland. However, large-scale implementation of such comprehensive data models remains computationally intensive and is often constrained by data availability.

2.2.2. Graph-Based Extensions of Visibility Analysis

Graph-based methods extend visibility analysis beyond isolated viewpoints to examine visual connectivity among multiple locations. Visibility Graph Analysis (VGA), rooted in space syntax theory (Hillier and Hanson, 1984; Hillier, 1996), models environments as 2D grids where nodes connect if their corresponding spaces are mutually visible (Turner et al., 2001). Metrics like mean depth and centrality describe spatial configuration and predict human movement patterns. While VGA is effective for structured indoor settings or defined outdoor areas, it inherits limitations from LoS-based methods: vertical complexity and environmental semantics are often oversimplified. To address these gaps, efforts continue to develop 3D visibility graphs (Varoudis and Psarra, 2014; Lu et al., 2019; Omrani Azizabad et al., 2024). For semantic enrichment, the Integrative Visibility Graph (IVG) incorporates functional nodes (e.g., food and drink facilities) (Natapov et al., 2013), while the Functional Visibility Graph (FVG) systematically links urban functions to spatial nodes via visibility edges, measuring visual accessibility to specific activities (Shen and Wu, 2022). Despite these advancements, existing graph-based methods remain grounded in geometric LoS

simulations when defining the visibility, which fall short of capturing human visual perception. In contrast, [Bartie et al. \(2015\)](#) introduces a novel approach to identifying landmark relationships from single images based on semantic similarity, presenting the potential to study the visibility and perception of landmarks beyond geometric constraints.

2.3. Street View Images as Proxy for Visibility Analysis

2.3.1. Visibility Analysis Centring on Semantic Elements

The emergence of SVI as an essential data source in urban studies brings a new paradigm of visibility analysis, the visibility of semantic elements and instances. Commonly collected along road networks by map service providers, SVI presents good organisation and availability in metadata, such as coordinates, heading and field of view ([Anguelov et al., 2010](#); [Hou and Biljecki, 2022](#)). With the convenience, SVI is commonly regarded as the visual proxy of human beings in the street environment ([Ito et al., 2024](#)). Relying on Computer Vision (CV) models, researchers can easily detect the pixels of buildings, trees, or designated object instances from SVI and calculate their existence ratio in the image frame. The pixel ratio, as a visibility metric, represents the extent to which the potential observer in the street environment perceives the element or instances. The Green View Factor (GVF), for example, is a metric of the perceived greenery element in streetscape, and is proven relevant to property price ([Yang et al., 2021](#); [Xu et al., 2025](#)), and mental health conditions ([Belcher et al., 2024](#)). Similarly, Building View Factor (BVF) and Sky View Factor (SVF) derived from SVI have become important metrics for describing urban canyon ([Hu et al., 2020](#)) from a human perspective, and play roles in Local Climate Zone (LCZ) classification ([Li et al., 2025](#)) and climate modelling ([Middel et al., 2018](#); [Fujiwara et al., 2024](#)).

Common use cases detect visual elements or instances in the foreground of SVI, as they are close enough to the camera, providing sufficient colour or texture details for CV recognition. However, the background pixels are often dropped and ignored. Elements concurring in the background are usually blocked by the foreground buildings or trees ([Fan et al., 2025](#)), or presented in low resolution, adding difficulty for machine detection. Nevertheless, it is argued that valuable messages are naturally embedded in urban objects' visible or invisible conditions in the image background. As a typical example, urban landmarks often appear in the background of a pedestrian's field of view, and their extent of presence is related to the attractiveness of the observation location or path ([Mor et al., 2021](#)). [Pyka et al. \(2022\)](#) used high-resolution LiDAR data to generate synthetic panoramas

and evaluated the visual exposure of landmarks as background elements, demonstrating the potential of image mediums for landmark visibility analysis.

2.3.2. *Imaging Lines of Sight via Visual-Language Models*

The development of Vision-Language Models (VLM) greatly lowers the barriers to acquiring and understanding urban information using visual data. VLM enable the natural establishment of correspondences between image data, such as satellite imagery and SVI and real-world semantics. Contrastive Language-Image Pre-training model (CLIP) (OpenAI, 2022), developed by OpenAI, is a typical example of VLM. The model takes images and their corresponding textual descriptions as input and learn to associate the knowledge from both modalities by computing the similarity between text and image embeddings and minimising contrastive loss (Radford et al., 2021). Applying the principles of CLIP, Klemmer et al. (2024) develops the ‘SatCLIP’ for matching geographic coordinates and visual characteristics extracted from satellite imagery. Huang et al. (2024) propose the ‘UrbanCLIP’, which infers urban functions using SVI and a fine-tuned CLIP model.

A more prevalent application of VLM is in zero-shot object detection, which allows searching and localising target objects in image space without additional pre-training or fine-tuning of the model. Well-known zero-shot object detection models include Grounding DINO (Liu et al., 2024) and OWL-ViT (Minderer et al., 2022, 2024). Both of them accept textual queries for searching the target, while OWL also allows image queries. It is assumed that urban landmarks, as distinct visual labels, can be detected naturally from SVI with a zero-shot detection model. The detection process can be regarded as ‘observation’ from machine vision at a specific SVI location. In this way, LoS towards landmarks and the meaningful visual context and connections can be identified, which defines the image-based visibility analysis method. The details of the method will be elaborated in the following sections.

3. Methodology

3.1. *An Image-based Landmark Visibility Detection Method*

Taking a landmark as an example, Figure 2 illustrates the workflow for assessing and mapping the visibility of target objects from panoramic SVIs. Key steps include relative positioning, image zooming, and object detection. Panoramic SVIs and metadata, including heading and coordinates, are retrieved from the Google Street View service.

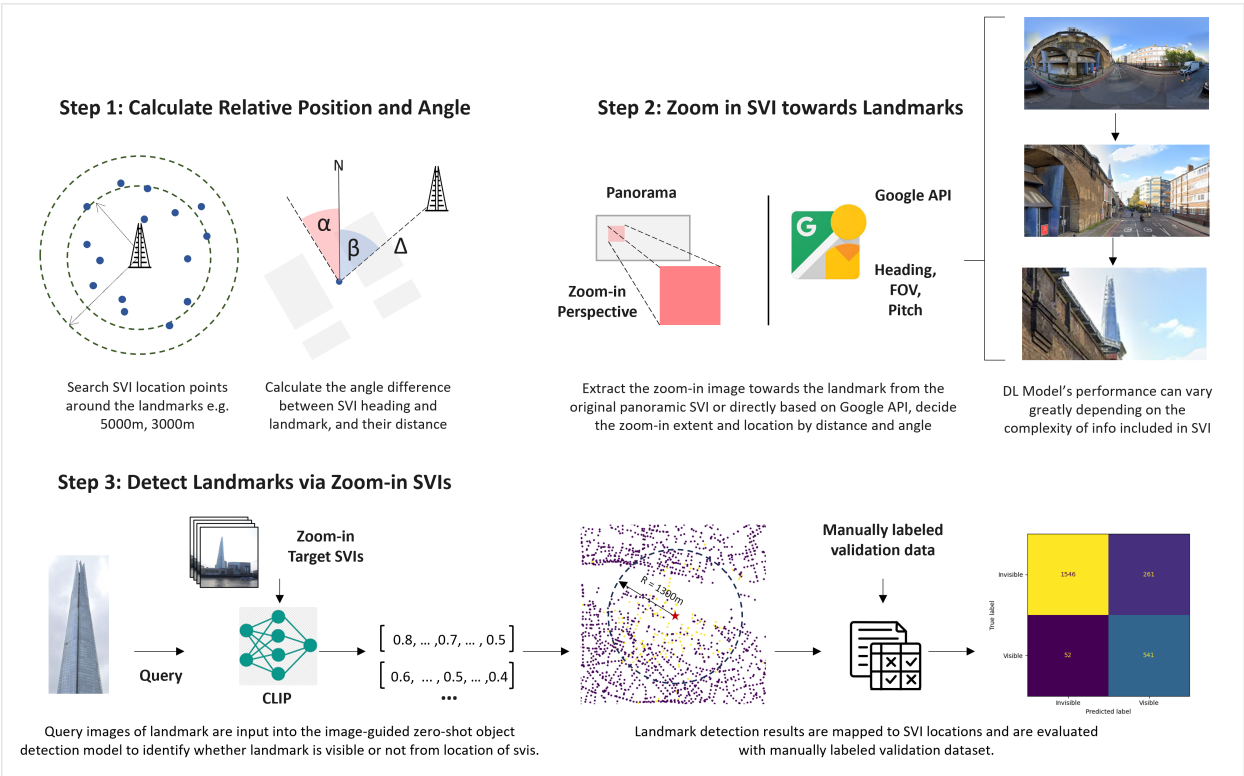


Figure 2: Workflow of locating and detecting the visibility of a distant landmark from SVI. Imagery: Google Street View, Wikimedia Commons.

3.1.1. Step 1: Calculate Relative Position and Angle

The process begins by identifying SVI location points within a set distance around a landmark (e.g. 3000m) as potential observers in the analysis. Once these SVI locations are selected, the distances and relative angles between the SVI locations and the landmark are calculated, which helps position the landmark in image space.

Let a panoramic SVI be at location $O = (x_o, y_o)$, the landmark at location $L = (x_\ell, y_\ell)$, both in the local projected Coordinate Reference System (CRS). The panorama has width W and height H_{img} in pixels, and heading h , clockwise from geographic north in radians. The landmark has a height H in meters. The Euclidean distance from the observer to the landmark is:

$$d = \|L - O\|_2 = \sqrt{(x_\ell - x_o)^2 + (y_\ell - y_o)^2}. \quad (1)$$

Using the planar axes convention (east x , north y), we can calculate the horizontal azimuth of the landmark compared to the observer from north as:

$$\alpha = \text{atan2}(x_\ell - x_o, y_\ell - y_o) \quad [\text{radians}]. \quad (2)$$

By converting both the panorama heading and landmark horizontal azimuth to degrees, we can calculate their difference and wrap to 0° – 360° . This quantity tells us how far to the right (0° – 180°) or left (180° – 360°) of the heading direction, the landmark lies in panoramic SVI.

$$\Delta\alpha^\circ = (\alpha^\circ - h^\circ) \bmod 360. \quad (3)$$

Because the panorama is stored in an equirectangular projection, the horizontal angle is linear in pixel column. With the horizontal angle difference $\Delta\alpha^\circ$, we can further calculate the horizontal pixel coordinate of the landmark on a panorama.

$$x_{\text{pix}} = \left(\frac{W}{2} + \frac{\Delta\alpha^\circ}{360^\circ} W \right) \bmod W. \quad (4)$$

3.1.2. Step 2: Zoom-in SVI Towards Landmarks

In the next step, the panoramic SVI is zoomed in towards the upper half of the landmark, which is commonly less blocked by other buildings. In this way, the landmark occupies a larger portion of the frame. It reduces the noise and complexity introduced by other visual elements that could affect the performance of the following object detection.

The zoom-in extent is determined based on the distance d between the SVI location and the landmark and the landmark’s physical height H . Specifically, the landmark’s elevation angle in an image is:

$$\epsilon = \arctan\left(\frac{H}{d}\right). \quad (5)$$

Assuming a full vertical field of view $\theta_v = 180^\circ$ and panorama height H_{img} (px), hence the landmark’s height in pixels is:

$$h_{\text{pix}} = \epsilon \frac{H_{\text{img}}}{\theta_v}. \quad (6)$$

Taking the horizon line (image mid-height) as the reference, the bottom and top of the extent are defined to focus on the upper half of the landmark. Occasionally, extra padding space can be added to the top of a landmark:

$$y_{\text{bottom}} = \frac{H_{\text{img}}}{2} - 0.50 h_{\text{pix}}, \quad y_{\text{top}} = \frac{H_{\text{img}}}{2} - 1.00 h_{\text{pix}}. \quad (7)$$

Let x_{pix} be the landmark’s central column obtained from the azimuth difference. Then the horizontal limits can be defined symmetrically:

$$x_{\text{left}} = x_{\text{pix}} - \frac{y_{\text{bottom}} - y_{\text{top}}}{2}, \quad x_{\text{right}} = x_{\text{pix}} + \frac{y_{\text{bottom}} - y_{\text{top}}}{2}. \quad (8)$$

The four bounds ensure a scale-consistent, nearly square zoom that adapts smoothly to landmark height and distance.

$$B = [x_{\text{left}}, y_{\text{top}}, x_{\text{right}}, y_{\text{bottom}}]. \quad (9)$$

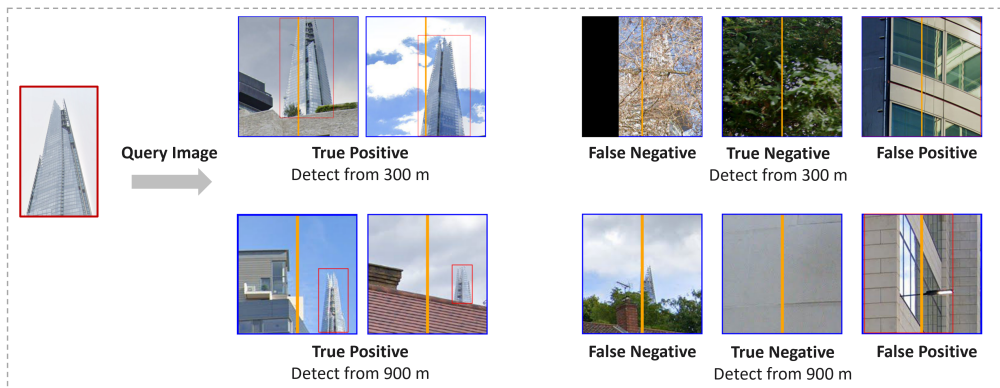
Figure 3a illustrates the attempts to locate The Shard, the highest building in the UK, in the image space of SVIs. The green line represents the heading of the camera, the yellow line represents the direction of The Shard relative to the SVI location, and the red and blue bounding boxes represent the space where the whole and the upper half of the building may occur on the image, respectively. It is observed that The Shard can be occasionally obstructed by other buildings in SVIs.

3.1.3. Step 3: Detect Landmarks via Visual-Language Model (VLM)

The study conducts zero-shot object detection on the zoomed-in SVIs to identify potential landmarks. The task is supported by Vision Transformer for Open-World Localisation (OWL-ViT) (Minderer et al., 2022), a model combining CLIP and lightweight object classification and localisation heads.



(a) A showcase of localisation boxes with landmark visible (first row) and blocked (second row). Imagery: Google Street View.



(b) Example results of true positive, true negative, false positive and false negative from landmark detection. Imagery: Google Street View, Wikimedia Commons.

Figure 3: Visualisation of the landmark detection process. (a) Locating landmarks using bounding boxes. (b) Detecting the landmark within the zoomed-in region.

Specifically, the study adopts the image-guided method supported by the model for landmark detection. A query image representing the recognisable visual features of the landmark is input to find the most similar visual object on the zoomed-in image. The detection process generates confidence scores that indicate the likelihood of the landmark’s presence in the images. Image queries perform much better than text queries, such as landmark name and shape description, when landmarks are partly obstructed in the complex street environment.

To evaluate the performance of the image-based visibility detection method, a validation dataset is generated for each landmark by dividing the total SVI locations into four distance bands from the central landmark and randomly sampling 100 locations per distance band. The sampled SVIs are manually audited and labelled with ‘visible’ / ‘invisible’ regarding the landmarks, using the open-source labelling platform of Label Studio (Tkachenko et al., 2020). The label distribution of the validation dataset is detailed in [Appendix B](#). A confusion matrix and metrics of Accuracy, Precision, Recall, and F1 scores are calculated to evaluate the method’s performance.

Figure 3b presents example results of detecting landmarks with OWL-ViT model. It is proven that the model can recognise The Shard building from 300m and 900m, with the proper zoom-in processing. Even so, different kinds of classification mistakes can occur. For example, the model may regard irrelevant buildings or components as The Shard itself. In some cases, though The Shard is shown in the image, most of them are blocked by trees in the foreground, which causes potential classification errors.

3.2. A Heterogeneous Graph Addressing Visual-Spatial Interaction

Utilising the visibility detection results, the study constructs a heterogeneous visibility graph to explore the visual-spatial interactions between SVI locations and landmarks, and landmarks themselves within the urban environment.

3.2.1. Graph Definition

Urban landmarks and SVI locations are defined as distinct node types. Edges are constructed between the same and different node types, respectively. As shown in the Figure 4, there are three different types of edges defined in the graph. For adjacent SVI nodes along the road network, undirected edges can be defined to represent their spatial proximity relationships. [Appendix A](#) elaborates on how to recognise effective proximity connections among individual SVI locations based on road network typology. Similarly, a landmark and an SVI can also be spatially adjacent. Undirected edges representing such spatial proximity are defined

between a landmark and its nearby SVIs within 50 m’s distance. Besides spatial proximity, visibility is important in understanding the interaction between different nodes. Directed edges representing visibility are defined from SVI nodes to landmark nodes, according to the landmark detection results. The heterogeneous graph is constructed using the Python packages of Deep Graph Library (DGL) (Wang et al., 2020).

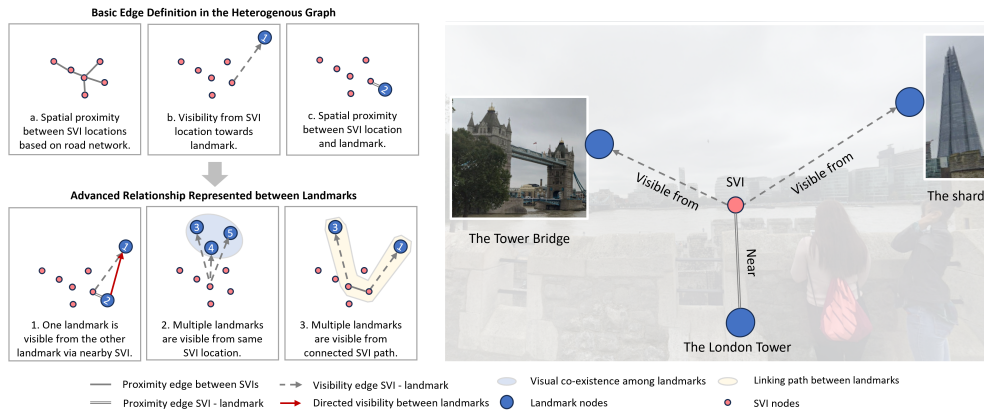


Figure 4: Left: Different types included in the graph definition. Right: An SVI taken near the London Bridge, showing how SVI can represent multiple edge relations via a single image. Imagery: Google Street View.

3.2.2. Advanced Relationship Represented by Graph

Three advanced relationships can be represented based on the node and edge definitions to describe more complex spatial and visual interactions between landmarks. These relationships are named as Inter-visibility, Visual Co-existence, Visible–Accessible–Visible (VAV) Path.

Inter-visibility. We define visibility between landmarks as the situation in which one landmark is visible from the site (nearby SVI) of the other landmark, one serving as the observing location and the other serving as the target object. As shown in Figure 4, an SVI taken near the London Tower, one of the most iconic landmarks in London, captures another famous landmark, The Shard, within its image content. Using SVI in proximity as a medium, we can investigate the inter-visibility relationship between any pair of landmarks.

Visual Co-existence. Beyond inter-visibility, Figure 4 reveals that multiple landmarks can be observed at the same location, representing a co-existence opportunity of specific landmarks in the visual environment. In the graph, it is represented as multiple visibility edges linked to one single SVI node. The more frequently the same group of landmarks is observed from different SVI locations, the stronger they create a united impression on the public.

Visible–Accessible–Visible (VAV) Path. The visual co-existence can be regarded as an extreme manifestation of the broader VAV pathway. In many cases, two landmarks may not be directly visible from the same location. Instead, they are connected via intervening street-level viewpoints and the road network. People build their visual impression of multiple landmarks through these pathways, and a disruption of some key pathways, not necessarily on the protected landmark viewpoints, could also undermine the connections between landmarks. Incorporating the visual co-existence, the VAV path provides a general method for quantifying the spatial-visual connections between landmarks.

4. Case Study

4.1. Visibility for Single Landmark and the Related Visual Context

Table 1: Iconic tall landmark structures investigated in the first case study, including both high-rise buildings and non-habitable towers. Imagery: Wikimedia Commons.

Landmark	The Shard	Petronas Towers	Tokyo Tower	Eiffel Tower	Taipei 101	Burj Khalifa
Query Image						
City	London	Kuala Lumpur	Tokyo	Paris	Taipei	Dubai
Height (m)	310	451.9	332.9	312	508	829.8
Built-up Year	2013	1998	1958	1889	2004	2010
Latitude	51.5045	3.1579	35.6586	48.8584	25.0339	25.1972
Longitude	-0.0865	101.7113	139.7454	2.2945	121.5645	55.2744

In the first case study, we aim to assess the effectiveness of the image-based visibility detection method and explore its potential in revealing visual context

during observation. We apply the proposed image-based visibility detection method to investigate the visibility of the most famous tall landmark structures in six global cities. The details of the landmarks are presented in Table 1. For each landmark, sampling points in a 30 m interval and within a 3000 m buffer are collected from OSM road network data. Coordinates of the points are used to retrieve the nearest SVI from the Google Street View service. Then, steps 1 - 3 introduced in Section 3.1 are applied to detect the visibility of landmarks from the corresponding SVI. We then compare the SVI-based visibility with visibility simulated from 3D urban models and visual interest reflected by the distribution of geotagged Flickr images.

4.1.1. SVI-based Visibility vs 3D Simulated Visibility

In the first step, we compare the image-based visibility results with the 3D simulated visibility results at SVI locations, by evaluating the classification accuracy metrics for ‘visible’ / ‘invisible’ with the same validation dataset created. We carry out 3D visibility simulation with the Python package of ‘VoxCity’¹ (Fujiwara et al., 2026). ‘VoxCity’ is a one-stop toolset for collecting and converting open 3D urban data to voxels, and conducting 3D spatial analysis based on them. 3D visibility simulation is carried out within a 3000-meter radius from each landmark, using a uniform 3D voxel grid size of $5 \times 5 \times 5$ m. The data models applied to generate voxels incorporate buildings, tree canopy and terrain, whose sources are detailed in Table C.5 in Appendix Appendix C. We employed different data sources for each city, depending on the sources’ specific geographic coverage areas. Furthermore, to explore the underlying differences between the two visibility detection methods, we examine the proportions of key street view elements, such as buildings, greenery, and sky, at locations classified as ‘only SVI visible’, ‘only 3D visible’, ‘both visible’, and ‘both invisible’. These street view elements are derived from semantic segmentation on SVI, supported by the Python package ‘ZenSVI’², developed by Ito et al. (2025).

4.1.2. SVI-based Visibility vs Flickr-based Visibility

In the second step, we collect geotagged images with landmark tags from Flickr, to recognise their distribution difference with landmark visibility derived from SVI. Crowd-sourced images from Flickr have been proven to have a strong association with public visiting towards urban space (Wood et al., 2013; Mor et al.,

¹<https://github.com/kunifujiwara/VoxCity>

²<https://github.com/koito19960406/ZenSVI>

2021) and landscape preference (Foltête et al., 2020). In this study, the distribution of Flickr images serves as a proxy of people’s interest in viewpoints towards landmarks. The Flickr images with landmark tags are searched with Flickr’s official API³, and within a 3000 m radius of the landmark.

To understand why people select or do not select specific view locations towards a landmark, we apply the Dice coefficient to describe the extent of overlap of the distribution of SVI and Flickr-based visibility in local space. Specifically, we summarise the quantity of landmark visible SVI locations and Flickr images within the local H3 grid and normalise them as proportions across all the grids. Then, Formula 10 is applied to calculate the Dice coefficient. A $Dice_k$ value of 1 indicates complete overlap of the two visibility proxies, and 0 indicates no overlap.

$$Dice_k = \frac{2 \min(P_{svi}(k), P_{flickr}(k))}{P_{svi}(k) + P_{flickr}(k)} \quad (10)$$

where:

- $Dice_k$ ranges from 0 to 1, indicating the extent of overlap between the two distributions.
- $P_{svi}(k)$ is the normalized proportion of SVI visibility in the H3 grid k .
- $P_{flickr}(k)$ is the normalized proportion of Flickr visibility in the H3 grid k .

With Dice coefficient, we further divide the local H3 grids into two groups: the tourism viewpoints ($Dice_k \geq 0.5$) and citizen viewpoints ($Dice_k < 0.5$). We compare the groups’ differences in a series of built-environment and socio-economic variables, including buildings and population density, street view features, Point of Interest (POI) density, and Airbnb density, rent price and available days. The first three groups of variables are derived from Urbanity, a global feature-rich network dataset developed by Yap et al. (2023). While the Airbnb-related data are retrieved from Inside Airbnb⁴, a project that collects and provides data about Airbnb’s impact on residential communities.

³<https://www.flickr.com/services/api/>

⁴<https://insideairbnb.com>

4.2. Multi-landmark Visibility and the Visual Interaction

In the second case, we explore our method’s potential in revealing complex visual structure and connections formed by multiple landmarks, and its value in heritage conservation. With the latest SVI collected from Google Street View, we investigate the visibility of 10 famous landmarks along the River Thames in London, UK, and aim to reveal their spatial-visual interaction with each other and with the street space. The landmarks are selected with reference to the review count ranking on Tripadvisor. The details and distribution of the landmarks are illustrated in Figure 5. After detecting visibility for each landmark with the proposed image-based method, we follow step 4 in Section 3.1 to build a heterogeneous graph. We conduct graph-based statistics to understand the direct and indirect visual connections among landmarks.

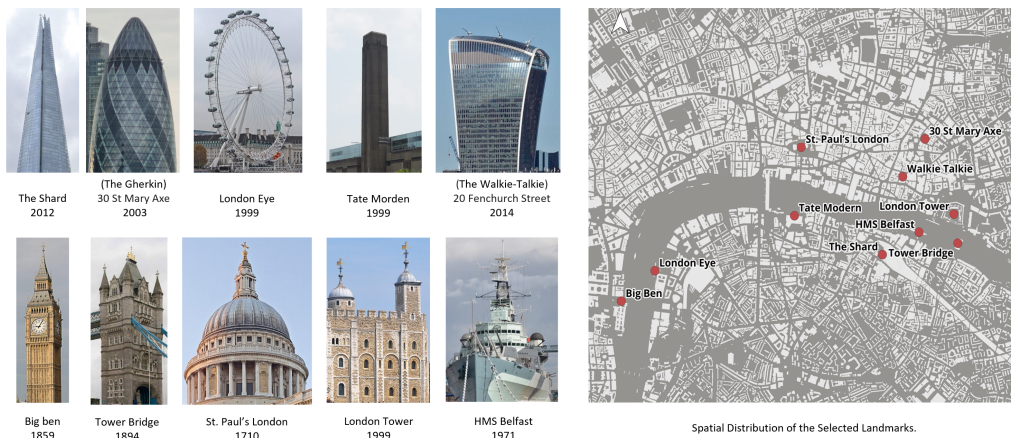


Figure 5: Left: Query images of different landmarks investigated in the second case study. Imagery: Wikimedia Commons. Right: The spatial distribution of the selected landmarks along the River Thames. Basemap: © OpenStreetMap contributors.

4.2.1. Different Roles of Landmarks in Riverside Landscape

A common experience applicable to the selected landmarks along the Thames River is that they are both part of the landscape and prominent viewing locations. However, little knowledge has been gained about whether a landmark serves more as a viewing point or as an observed object in urban settings. The inter-visibility relationship between landmark nodes is measured to answer the question. The differences in the roles of modern and historical landmarks are further discussed.

In urban sightseeing, beyond direct inter-visibility, people often experience multiple landmarks appearing together [Lopes et al. \(2019\)](#). Some landmarks are frequently seen together, which reinforces their visual connection in the public’s perception, while others tend to appear in isolation, emphasising the unique identity of specific local spaces. To analyse this, we summarise the frequency and form in which landmarks are included in the visual co-existence relationship.

4.2.2. *Visual Connection between Landmarks: Path and Strength*

To generalise the visual co-existence relationship to any landmark pairs, we apply the random walk algorithm ([Pearson, 1905](#); [Xia et al., 2020](#)) to identify the VAV paths linking different landmarks. Specifically, starting from a random SVI location that is visible to one landmark, the algorithm randomly explores the road network for a fixed number of steps. The search terminates when it reaches a visible point of a different landmark. An angle penalty strategy is applied in the path search process to avoid U-turns, ensuring smoother transitions and more realistic connectivity. By normalising the count of valid paths between any two landmarks with the total number of walks, we obtain a measure of connection strength that can be compared across landmark pairs. Furthermore, we identify the important and vulnerable corridors that play significant roles in connecting different landmarks. The corridors serve as valuable guidance for local planners to maintain the existing perceptual patterns of landmarks.

5. Results

5.1. *Effectiveness of Image-based Visibility Analysis*

Figure 6 presents the distributions of SVI locations detected as visible to the corresponding landmarks. The distributions are compared with two other visibility proxies: visibility simulated with 3D models and the distributions of Flickr images with the landmark tags. For 3D simulated visibility, it is initially represented based on 5×5 m grids. Grids identified as visible are joined spatially to the SVI locations for comparison.

Overall, landmark-based visibility and 3D simulated visibility share more similarities in spatial distribution. In particular, the visible location distributions in Paris, Tokyo, and Dubai are highly similar in both extent and density. In Kuala Lumpur, London, and Taipei, the 3D simulation method detects significantly more visible locations than the SVI-based approach. In contrast, the spatial distribution of Flickr images reveals a distinct pattern. Around the landmarks, the Flickr image

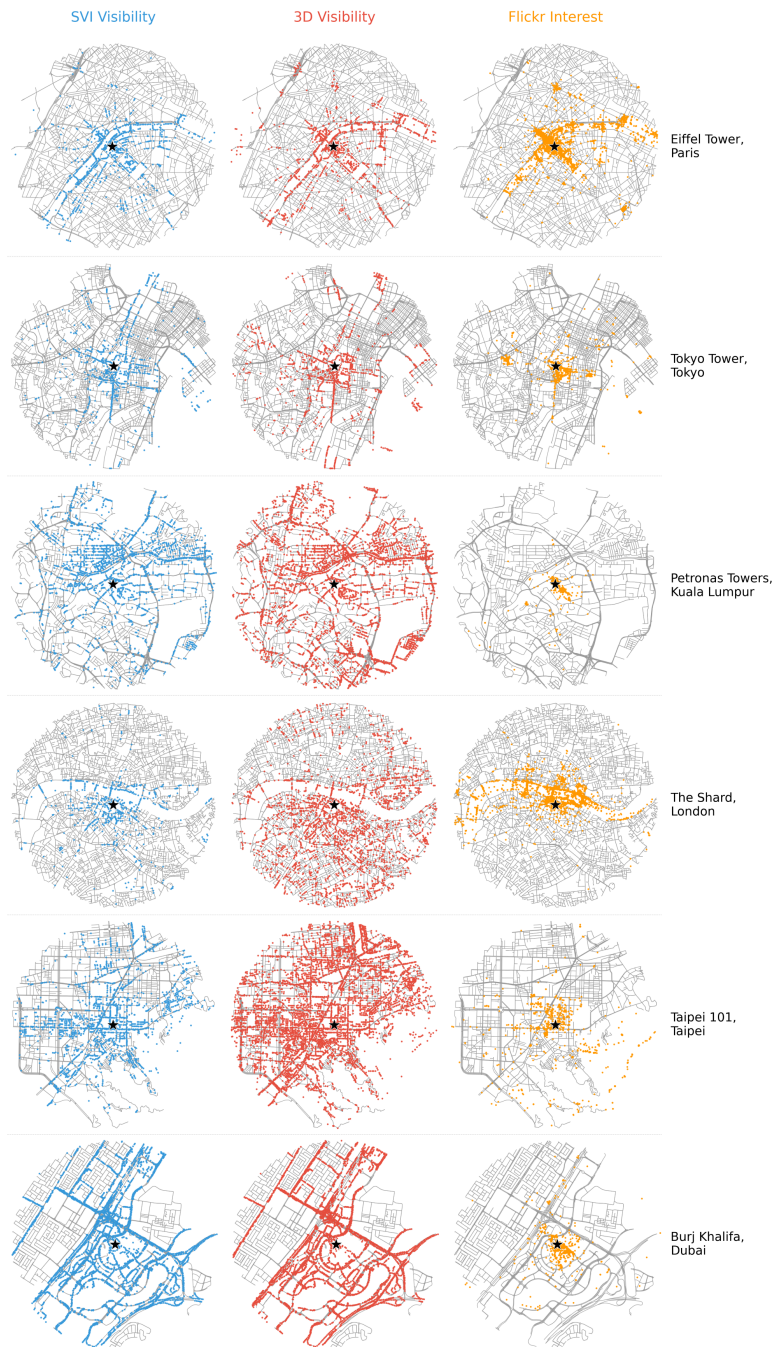


Figure 6: A comparison of distribution for SVI-based landmark visibility, 3D simulated landmark visibility, and Flickr images with landmark tags. Basemap: © OpenStreetMap contributors.

distribution is more centrally focused and compact. Beyond these visual distribution comparisons, this section employs a series of quantitative analyses to reveal the differences between SVI-based visibility and the other two visibility proxies.

5.1.1. Comparing SVI-based Visibility with 3D Simulated Visibility

To validate the effectiveness of the proposed image-based visibility detection method, we compare the performance of image-based visibility detection and 3D model-based visibility simulation on the validation dataset. The result is summarised as in Table 2. The validation set is composed of 2400 locations from the six cities, and is manually labeled as visible or invisible to the corresponding landmarks. Compared to the 3D-based method, image-based method presents overall higher accuracy, and better precision and recall scores in classifying both visible and invisible samples.

Table 2: A summary of performance for image-based visibility detection and 3D model-based visibility detection.

Class	Support	Image-based Visibility Detection			3D Model-based Visibility Simulation		
		Precision	Recall	F1-score	Precision	Recall	F1-score
Invisible	1807	0.9675	0.8556	0.9081	0.929	0.7023	0.7999
Visible	593	0.6746	0.9123	0.7756	0.4797	0.8364	0.6097
Accuracy			0.87			0.74	

To gain a more detailed observation of both methods, Figure 7a summarises their precision for visible and invisible classifications across different landmarks and at different distance bands.

More details about the methods’ performance are attached in Appendix D. For most landmarks, the SVI-based method presents best performance in identifying visible locations in the distance band of 0 - 500 m, with precision scores for most landmarks around and above 0.8. Identifying visibility to the Eiffel Tower achieves a highest precision of 0.98. The precision scores can drop significantly as the distance increases. For locations within the distance band of 500 - 1000 m, the precision scores drop to around 0.6 for landmarks of the Eiffel Tower, Burj Khalifa, Petronas Towers, and Taipei 101. For Tokyo Tower, the precision dropped to 0.24. As an exception, performance for detecting visibility for The Shard doesn’t change significantly. Though performance degrades as distance increases, the SVI-based method still outperforms the 3D-based method in all the distance bands in terms of the precision of detecting visible locations.

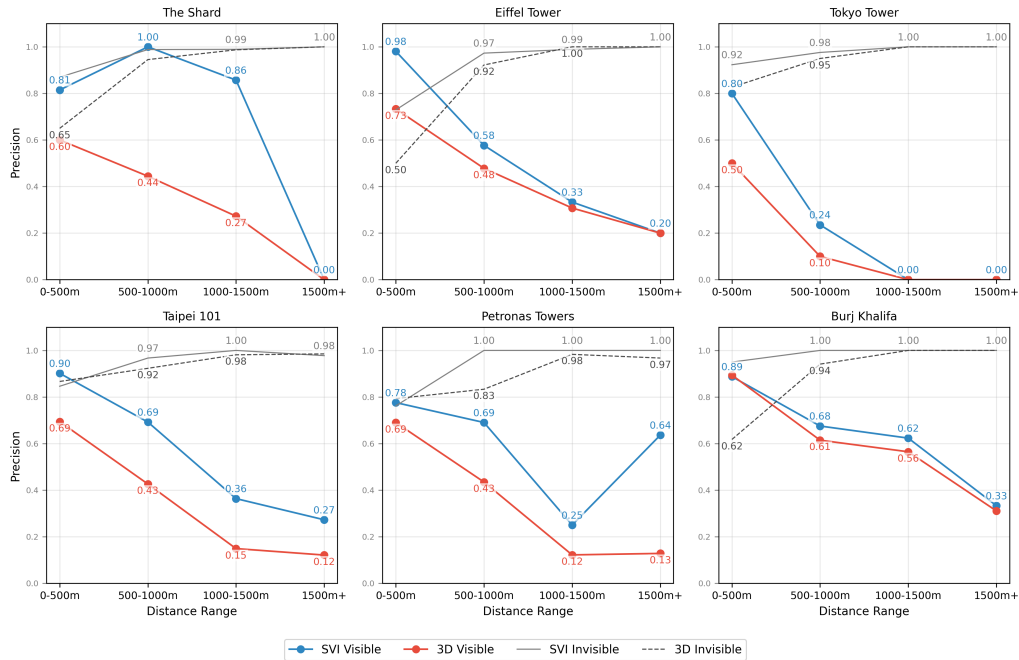
For identifying invisible locations, both methods achieve higher precision, and the pattern is prevalent across distance bands. The reason is that the proportion of invisible locations is naturally higher in the validation set and across landmarks. As distance increases, the proportion difference gets amplified further, and the impact of misclassified samples on the precision calculation tends to be reduced.

To further explain the difference between SVI-based and 3D-based visibility detections, Figure 7b illustrates how the visibility detection outcomes relate to the visible semantic elements of vegetation, sky, and construction in the foreground. SVI locations are reclassified into ‘Both Invisible’, ‘Both Visible’, ‘3D Only’, and ‘SVI Only’. Grouped with the classification, box-plots on the right side illustrate the distribution difference of semantic elements of vegetation, sky and construction, across different landmarks. As a showcase, on the left side, the spatial distribution of the classifications is mapped for the Eiffel Tower.

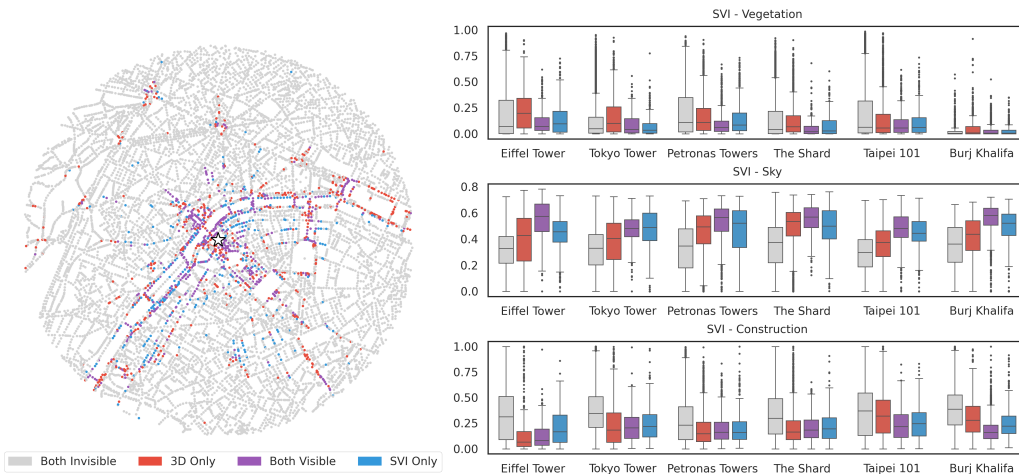
Both methods consistently demonstrate that areas where landmarks are visible tend to be open spaces. These areas are characterised by a significantly higher visible sky ratio and lower construction and vegetation ratios. In contrast, regions where landmarks are not visible typically present a more confined and crowded visual scene, with comparatively higher visible construction ratios. This overall trend reflects a general urban visual pattern that transcends the differences in the detection methods.

Compared to locations detected visible only by the 3D method, those only identified as visible via SVI generally exhibit less vegetation obstruction. This discrepancy is particularly pronounced in observations toward landmarks such as the Eiffel Tower, Tokyo Tower, and The Shard. This finding suggests that the SVI-based method more effectively considers tree obstructions, a factor not as well captured by the conventional 3D approach. At the same time, the construction ratios at SVI-detected locations do not show a lower trend compared to those from the 3D method. This justifies that the SVI approach is not biased toward low-density building areas; it can handle complex and crowded urban environments with notable built obstructions.

Beyond the quantitative difference above, 3D simulations classify a location as visible if it has a line of sight to even a small fragment of a landmark, which may not be recognisable as such in the SVI-based method. This potential overestimation in 3D simulations highlights the advantage of our SVI-based method in detecting only recognisable landmarks.



(a) Line plots comparing the precision of landmark visibility detection based on image and 3D methods, across different landmarks and distance bands.



(b) Left: Spatial distribution of match and mismatch locations between SVI-based visibility and 3D-based visibility for the Eiffel Tower. Right: Box-plots illustrating the proportion of semantic elements in the foreground of the views.

Figure 7: Plots comparing the performance and foreground visual element difference in SVI-based and 3D-based visibility detection.

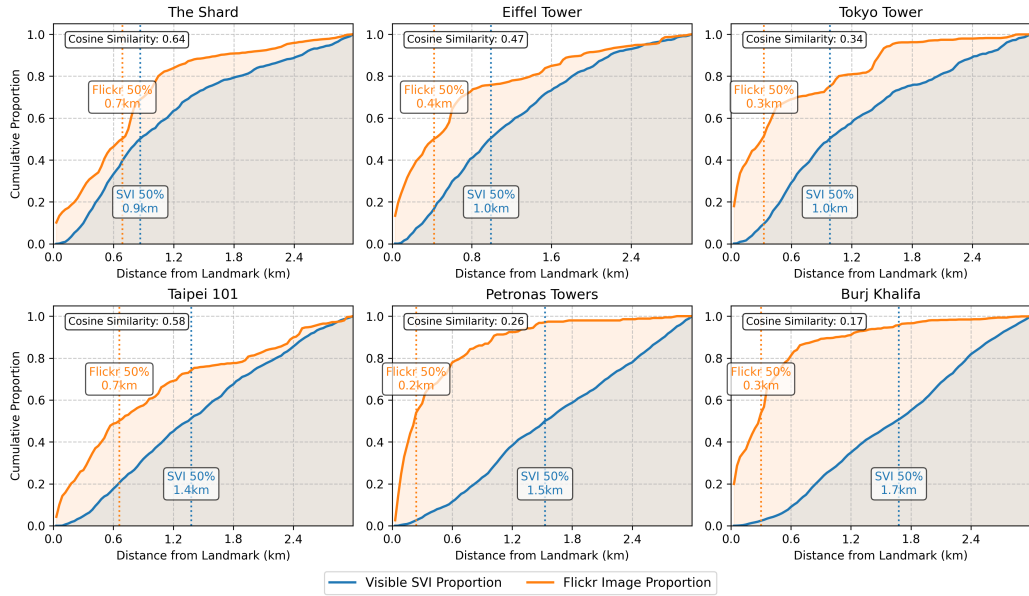
5.1.2. Comparing Landmark Visibility and Visual Interest

By validating the SVI-based visibility with ground truth, we prove that the SVI-based method provides a more reliable and objective distribution of landmark-visible locations in the urban environment. The locations suggest how general citizens can view and perceive landmarks in their everyday lives. In contrast, locations of landmark-tagged Flickr images reflect how landmarks are more likely to be perceived (and recorded) from the perspectives of tourists and photographers, as an explicit visual interest distribution towards the landmarks. A comparison between SVI-based visibility and the Flickr-based visibility can help define the socio-economic context brought by the SVI-based visibility.

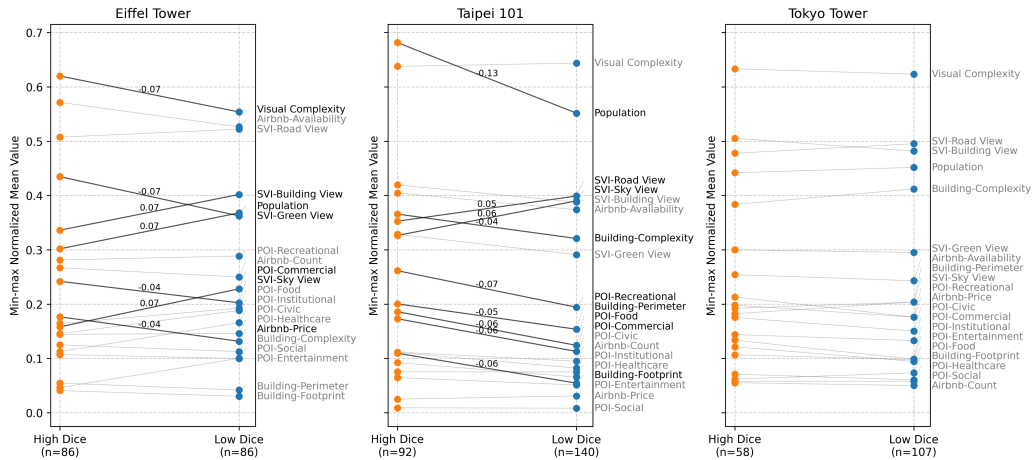
Figure 8a compares the cumulative proportion distribution of landmark-visible SVI locations and Flickr images along the distance from the corresponding landmarks. It is revealed that for The Shard, Eiffel Tower, Tokyo Tower and Taipei 101, both visibility proxies decline rapidly with increasing distance and exhibit similar patterns. Though the cumulation of Flickr images is generally faster, this alignment pattern suggests that the distances at which landmarks are visible from street locations are almost the distances where people tend to photograph or appreciate these landmarks. For The Shard, the cumulative distributions of landmark-visible SVI and Flickr images align most closely, indicated by the highest cosine similarity between curves. There is also a smallest difference between distances where the cumulative proportion of two indicators reaches 50%

In contrast, the Petronas Towers and Burj Khalifa exhibit a different pattern. Most Flickr images tagged with these landmarks are concentrated around the buildings, within a 500 m radius. However, the objective visibility derived from SVI is more evenly distributed over distance, with most visible locations appearing beyond 1000 m from the landmarks. This significant discrepancy further indicates that tourists and residents may perceive landmarks differently. Residents, who navigate the city in everyday life, can observe landmarks without physically approaching them, while tourists capture many photos close to the landmarks, reflecting a perception that relies on actually visiting the sites.

Dice coefficients are calculated to further measure the overlapping extent of the two proxies within local H3 grids. Maps illustrating their spatial distribution are attached in Appendix D. With Dice coefficients, we divide local areas with visibility to landmarks as tourism viewpoints ($Dice_k \geq 0.5$) and citizen viewpoints ($Dice_k < 0.5$), and compare their street view characteristics, POI and population density, built environment density, and Airbnb listing density and prices, with results presented in Figure 8b.



(a) Accumulated proportion distribution of landmark-visible SVI locations and Flickr images along the distance from the corresponding landmarks. The distances where the cumulative proportions reach 50% are labelled.



(b) Slope plots illustrating the socio-economic variables between tourism viewpoints and citizen viewpoints. Annotations are displayed only for paired variables with statistically significant differences at the 0.05 significance level according to the one-sample T-test.

Figure 8: Plots illustrating the distribution difference of landmark-visible SVI locations and Flickr images and the related socio-economic context.

According to the analysis, the Eiffel Tower, Taipei 101, and Tokyo Tower present different roles as the famous landmarks in their corresponding urban settings. For the Eiffel Tower, as suggested by Figure 8a, the visible location and visual interest align well in the space. The views of the Eiffel Tower can be regarded as more ‘stylised’, as they are significantly high in visual complexity, with more green views and sky views and fewer building views in the tourism viewpoints, suggesting that observations can commonly happen in open and designed spaces. Additionally, the tourism viewpoints also see significantly higher Airbnb prices but fewer commercial activities.

However, a similar pattern is not observed from the views of Taipei 101. Tourism viewpoints to Taipei 101 are featured with higher built environment density and complexity, more population and servicing POIs, which suggest a more crowded environment, accompanied by a stronger sense of commercialisation. In contrast, the citizen viewpoints present more open but loose environments, with higher sky and road view ratios. Compared to the Eiffel Tower, whose views from tourists and citizens present different characteristics, the views to Taipei 101 seem not specially designed, but follow the spatial concentration of population and functions. Additionally, there is no significant difference in the variable distribution between the tourism viewpoints and citizen viewpoints for Tokyo Tower. According to the analysis, it is inferred that the alignment between objective visibility and visual interest, and the observing context difference between tourism and citizen views, can be helpful tools to identify whether a landmark is well designed and incorporates organically with the surrounding urban environment.

5.2. Uncovering Visual Connection and Interaction Among Landmarks

In Section 5.1, we demonstrated the reliability of SVI in capturing the visibility of individual landmarks and its unique potential to reveal the visual context. Using 10 famous landmarks along the River Thames in London, in this section, we examine SVI’s ability to assess their visual relationships with one another and their interaction with street space driven by visibility.

5.2.1. Inter-visibility and Visual Co-existence

We begin by identifying inter-visibility between pairs of landmarks. Landmark A is considered visible from another landmark B if an SVI location within 50 m of landmark B captures landmark A. If the reversed condition is true, the two landmarks can be defined as inter-visible at street level, indicating a strong spatial connection. Figure 9 illustrates how inter-visibility delineates relationships among

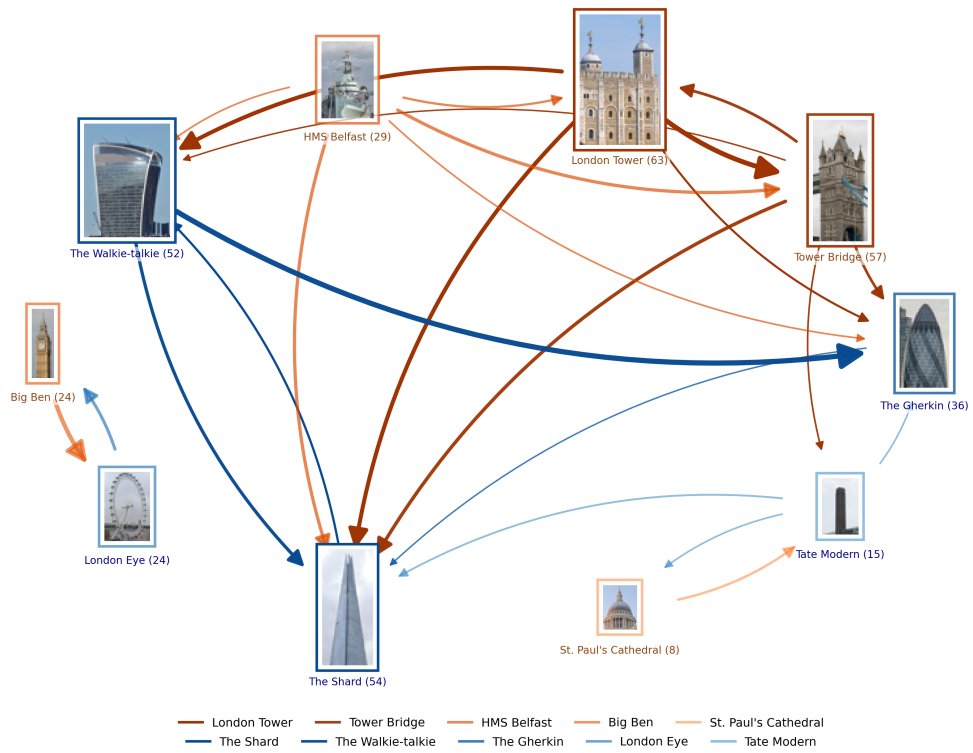


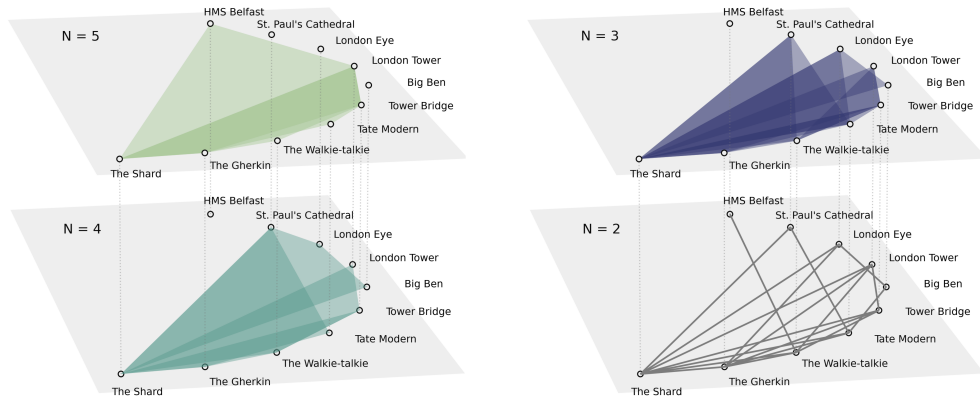
Figure 9: Inter-visibility between modern and historical landmarks along the River Thames, based on their location and height. Imagery: Wikimedia Commons. Software: NetworkX (Hagberg et al., 2008).

multiple landmarks. Arrows indicate the viewing direction, and their widths represent the frequency of visibility. The size of each landmark image corresponds to its prominence within these relationships. It is revealed that The Shard and The Gherkin are more commonly part of the visual landscape viewed from other locations. However, in the surrounding street locations of the two landmarks, fewer other landmarks can be observed. In contrast, the area near The Walkie-Talkie and HMS Belfast serves as a vantage point with good views of other high-rise landmarks. London Tower and Tower Bridge can be regarded as important visual hubs, functioning both as key observation points and as primary objects of observation. St Paul's Cathedral and the Tate Modern, as well as Big Ben and the London Eye, have formed inter-visible landmark pairs. Nevertheless, their visual relationships with other landmarks are relatively weak due to location and height limitations.

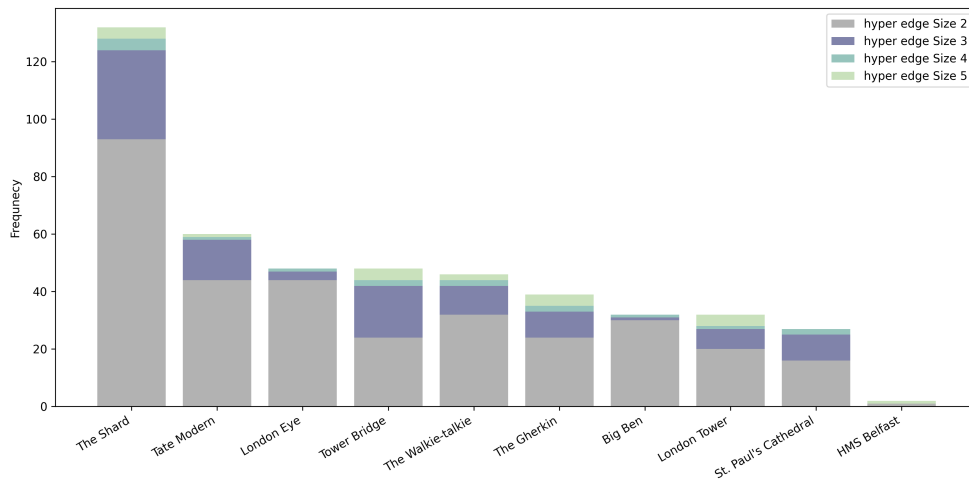
Beyond inter-visibility, visual interactions among landmarks can occur even beyond their immediate locations. We explore the concept of visual coexistence, which refers to the phenomenon where two or more landmarks are visible simultaneously from the same street locations. When certain landmarks are frequently viewed together within an urban area, it indicates not only intrinsic connections among the landmarks as objects of observation, but also their collective association with street space as symbols of heritage or important skylines. Figure 10 illustrates the various modes in which visual coexistence occurs among landmarks in the case study area. Notably, The Shard appears to be the most recurrent landmark, frequently co-occurring with others, presenting its central role in the current visual landscape along the River Thames. The other commonly co-occurring landmarks include Tower Bridge and London Tower, St Paul's Cathedral and London Tower, The Walkie-Talkie and The Gherkin. However, several landmarks rarely show together at street-level observation, such as the London Eye and The Walkie-Talkie.

5.2.2. *Linking Path and Strength based on Visual Co-existence*

Visual co-existence can still be regarded as an extreme scenario where landmarks are perceived and experienced in daily life, as it is defined only at fixed locations, ignoring the dynamic nature of human movement within the street network. Instead, the 'visibility-accessibility-visibility' (VAV) pathway provides a generalisable method to quantify the visual-spatial connections between landmarks and their combined impact on street space. A VAV path is defined as a random and natural path linking two SVI locations with visibility to different landmarks. When the path length is zero, the start and end locations are merged, representing visual



(a) Forms of visual co-existence (hyper-edge) that landmarks are included in.



(b) Frequency of landmark under each visual co-existence (hyper-edge) type.

Figure 10: Forms and frequency that landmarks are included in visual co-existence relationship. Software: XGI (Landry et al., 2023).

co-existence. The count of valid VAV paths between two landmarks measures their linking strength. The paths are searched using a random walk method. For each landmark, 2000 rounds of search are conducted. The search starts from a randomly selected SVI location visible to the landmark and ends when an SVI location visible to another landmark is found. The maximum step count in a path is set to 80.

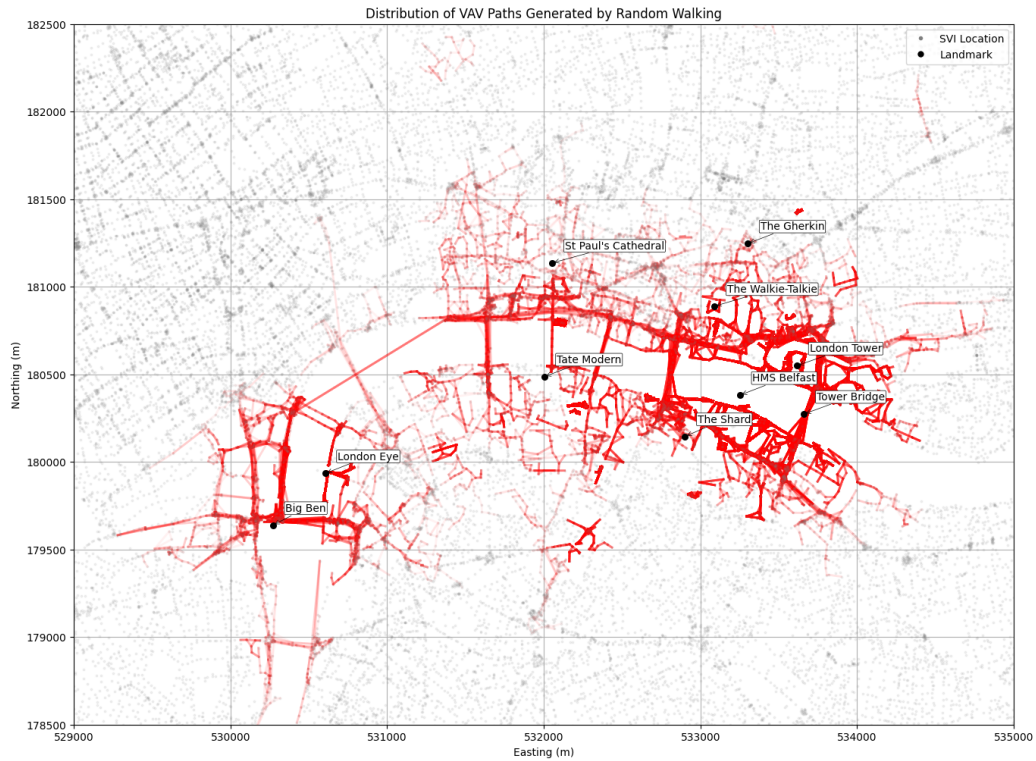
As shown in Figure 11a, the map illustrates the total paths searched for ten landmarks. It was found that most of the paths concentrated around a circle on the east side of the case study area. The paths link landmarks such as The Walkie Talkie, London Tower, Tower Bridge, and The Shard, filling the surrounding space's riverside pedestrian walks and main roads.

Beyond the circular area, there are lower-level hot spots centred around St Paul's Cathedral and the Tate Modern, and around the London Eye and Big Ben. Strong and concentrated linear linking paths are observed between the St Paul's Cathedral–Tate Modern hot spot and the eastern circle on the northern bank. However, these paths are truncated at the western ward boundary of the City of London and do not extend further west. In contrast, linking on the southern bank is more diffuse. No single, strong, concentrated path is observed on the southern bank that links either Big Ben–London Eye or St Paul's Cathedral–Tate Modern with the eastern landmarks. Instead, multiple linking paths are evenly distributed on the road network in the wards of Bishop's, Borough and Bankside, representing a more casual integration of landmarks into the visual background.

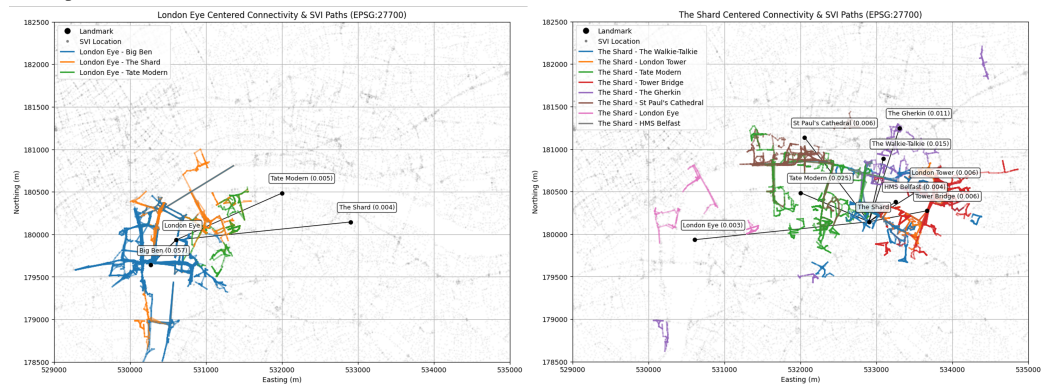
In addition to the patterns above, bridges on the River Thames serve as vital spatial and visual corridors for linking the landmarks. Over 29% of the total paths pass through the bridges. Specifically, if London Bridge were removed from the River Thames, 6.7% of the current VAV paths would be cut off, significantly reducing the linking between Tower Bridge, The Talkie Walkie, The Shard and Tate Modern.

Figure 11b presents the linking paths originating from specific landmarks, the London Eye and The Shard, and the accumulated linking strength between origins and destinations. The London Eye is closely tied with Big Ben in visual perception, both through inter-visibility and visual co-existence. The longest VAV path can extend south along the River Thames, passing over Lambeth Bridge. It is also capable of establishing an intermediate visual connection between the London Eye and The Shard based on visual co-existence, although they are nearly on opposite sides of the southern bank.

Regarding The Shard, the landmark exhibits the strongest visual connection with the Tate Modern, which commonly serves as a foreground object when The



(a) Accumulated VAV paths searched via random walk algorithm for 2000 rounds. A VAV path is considered valid when its endpoints are SVI locations that reveal different landmarks.



(b) Accumulated VAV paths originating from the London Eye and The Shard, and the landmarks linking strength to other landmarks. Only landmark pairs with linking strength over 0.002 are visualised.

Figure 11: VAV paths searched with random walk analysis.

Shard is observed in the background. This is followed by its strong link with The Gherkin and The Walkie Talkie, both high-rise landmarks. It is also noted that the visual interaction between The Shard and The Gherkin can occur at locations far from both landmarks, indicating their consistent roles as key elements of the urban skyline. Additionally, the linking strength between The Shard and St Paul’s Cathedral, London Tower, and Tower Bridge is similar, nearly double that of the London Eye. For these traditionally recognised London landmarks along the River Thames, The Shard, as a relatively new construction, serves as a closely related background element in views of them.

6. Discussion

6.1. An Image-based Framework for Visibility and Visual Relationship Analysis

Our study proves SVI as a sufficient medium for sensing distant space and capturing the ubiquitous connection and interaction between visual objects. Table 3 summarises its advantages and disadvantages compared to traditional 3D-based methods in visibility analysis.

Compared to 3D methods, the SVI-based method exhibits overall higher accuracy for detecting the visibility of each landmark. There is also better robustness with the increase of observation distance. The relative advantages of the SVI-based method come from two sources: Firstly, SVI generally presents better availability compared to high-quality 3D model data, especially in the urban realm. Though multiple openly available 3D model datasets exist, they are not always even in data quality or suitable for 3D visibility analysis in urban environments due to resolution or completeness limitations. Like the cases in Taipei and London, height data presents relatively low completeness in the corresponding building dataset. Secondly, sensing and perception based on SVI consider more real-world details, such as obstructions from trees, extended building roofs and billboards. Compared to the 3D method that simulates visibility as a geometric intersection, the image-based method respects the shape, texture, and other recognisable visual features of the object, reflecting a more grounded perspective.

The unique value of SVI-based method is further reflected in the contextual information it can bring for observation. Specifically, on the one hand, the visual content reflected in SVI is strongly linked to where the SVI is captured. Observation locations’ physical and socio-economic features introduce a spatial context of visibility, but are rarely realised and investigated in previous methods. On the other hand, image as a medium can naturally include multiple visual objects in one

view, which suggests their potential relationship, such as the foreground and background, and co-existence or isolation. The inter-object relationship introduces a dimension beyond geometry, and relates the visibility of target objects with wider semantic information, such as urban function and culture.

Table 3: A summary and comparison of advantages and disadvantages of different visibility analysis methods.

	3D-based Visibility	SVI-based Visibility
Pros	<ol style="list-style-type: none"> 1. Better spatial continuity of results 2. Higher computation efficiency 3. Flexibility in modifying models 	<ol style="list-style-type: none"> 1. Higher analysis accuracy/robustness 2. Aware of observation context 3. Detecting human-recognisable features
Cons	<ol style="list-style-type: none"> 1. Model resolution and availability limits 2. Incomplete consideration of semantic details and other urban themes, e.g., vegetation 	<ol style="list-style-type: none"> 1. Image resolution and metadata limits 2. Limited availability beyond street space and in rural areas
Applications	<ol style="list-style-type: none"> 1. Nature and urban environments 2. Simulation and evaluation of the planning and construction impact 	<ol style="list-style-type: none"> 1. Complex urban environments 2. Evaluating the visual condition of existing construction

Though with the advantages above, the application of the SVI-based method is restricted to the availability of SVI data. The objects to observe are also fixed, which should be existing buildings or constructions. The SVI-based method can only be used to evaluate rather than simulate the visual impact. In these cases, the 3D-based method presents better flexibility. In addition, effective observation via SVI depends on the image resolution, metadata quality, and power of the CV model – a similar condition also applies to observation based on well-functioned human eyes. Beyond a certain distance, or under poor lighting conditions, it is not feasible to recognise landmarks via both human and machine vision.

6.2. *A New Gate to Comparative Urban Research and Heritage Conservation*

Just as tourists discover a city through its iconic landmarks, researchers can decode urban development by examining how these landmarks interact with their surroundings. Our case studies, applying image-based visibility analysis to tall landmark structures across global cities and both modern and historic landmarks within London, demonstrate the methods’ great potential in comparative urban research and heritage conservation.

On the one hand, different roles and perception patterns are recognised for iconic landmark structures in global cities. For Petronas Towers in Kuala Lumpur and Burj Khalifa in Dubai, the landmarks are over 400 m in height and gain wide visibility from vast urban locations. The objective visibility of the landmarks

far exceeds the spatial extent of visual interest captured on Flickr, resulting in a singular, radiating visual positioning. The landmarks serve not just as local attractions but as integral components of the broader visual background. In contrast, in cities such as London, Tokyo, and Paris, the visibility around selected landmarks is effectively confined within well-defined spatial boundaries, such as along riverbanks or principal urban axes and primary roads. Concerning the urban fabric, the landmarks exhibit a more harmonious visual positioning, contributing to the spatial structure and distinctive characteristics of local areas. Furthermore, our analysis reveals varying perceptual drivers and contexts of the landmarks. For example, the view of the Eiffel Tower can be regarded as more 'stylised' from tourism viewpoints, while a similar pattern is not observed for Tokyo Tower. With the perception patterns revealed above, our research provides a novel perspective for evaluating the spatial impact of globally recognised landmarks. It offers further opportunities to improve the design quality and vitality of landmark-related space.

On the other hand, by employing a heterogeneous visibility graph to examine the mutual relationships among London landmarks and SVI locations, our method effectively captures the complex landscape patterns by multiple urban landmarks, a critical aspect for heritage preservation. First, our method clarifies the visual impact of new urban landmarks by showing how they integrate into the established network of traditional icons. For instance, when examining high-rises built in the past 25 years, such as The Gherkin, The Walkie Talkie, and The Shard, our analysis reveals their distinct roles relative to classic landmarks like St Paul's Cathedral, Tower Bridge, and Big Ben. These roles include serving as observation points, being observed, or frequently contributing to the visual background, as indicated by inter-visibility and visual co-existence patterns. Moreover, by combining visibility with accessibility using VAV paths, we can discern how urban landmarks that do not interact visually in a direct manner, such as Tower Bridge and the London Eye, establish indirect connections through unexpected spaces. This analysis not only calculates overall connection strength but also pinpoints the key locations and corridors facilitating these links, which have been proven to play positive roles in human way-finding tasks ([Omer and Goldblatt, 2007](#)).

In summary, unlike traditional heritage preservation planning, which focuses solely on the visibility of select landmarks from fixed viewpoints, our image-based visibility method enables the identification and protection of complex interconnections among landmarks, in terms of form, extent, and location. This approach has demonstrated significant promise for Heritage Impact Assessment (HIA), especially in dynamic urban environments ([Ashrafi et al., 2021](#)). Our work

also extends the exploration by [Shen and Wu \(2022\)](#) and [Natapov et al. \(2013\)](#) on semantics-enriched visibility graph.

6.3. *Limitations and Future Work*

There are several limitations in this study. To achieve a trade-off between performance and memory usage, our study prevents the usage of over-complicated Visual-Language Models (VLMs), such as GPT 4o ([OpenAI, 2024](#)), Qwen-VL ([Bai et al., 2023](#)), CogVLM ([Wang et al., 2024](#)). Integrated with multi-modal capability from Large Language Models (LLMs), these models generally achieve better performance in zero-shot detection, and also advance in other tasks such as Visual Question Answering (VQA) and image captioning. However, the additional functionality increases dramatically the model size and the cost for calling and inference, which is unnecessary for elaborating the proposed image-based visibility method. Nevertheless, it is promising that more advanced VLMs can help boost the capability of identifying visual objects beyond iconic landmarks, generalising the visual graph analysis to any named places and their visual features. Moreover, limited to the scope of the study, the usability exploration of the visibility graph, specifically integrating visibility into a road-based spatial network, is not sufficient. Our study reveals that visibility often represents a hyper-space relationship, which naturally complements the classical spatial model defined on spatial proximity and fits well with the graph structure. As a future direction, we can apply the relationship in use cases such as building height prediction, geo-localisation, urban environment embedding, and utilising graph deep learning methods.

7. Conclusion

With SVI and zero-shot object detection as a new basis for identifying the classical Line of Sight (LoS) relationship, the study proposes a novel visibility analysis method and allows space for analysing and revealing broader visual and spatial contexts of observation. Further, a heterogeneous visibility graph is constructed to address the complex relationships and interactions among visual objects and quantify their connection strength. Using two case studies to investigate the visibility and visual relationship of urban landmarks, the study presents our methods' reliability and wide application in urban design and heritage conservation. Specifically, the image-based visibility analysis fills the gaps in traditional 3D-based visibility methods, such as the limited availability of high-resolution 3D

data, a lack of human-centred perspective, and weak reliability and interpretability. Furthermore, the proposed visibility graph showcases the possibility of revealing the prevalent connection of any visual objects in the urban environment, benefiting computational social science and urban system research.

Appendix A. Integrating SVI Locations into Graph with Road Connection

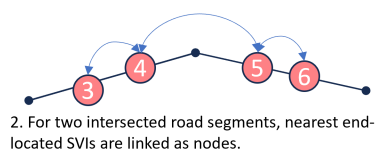
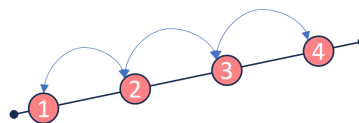
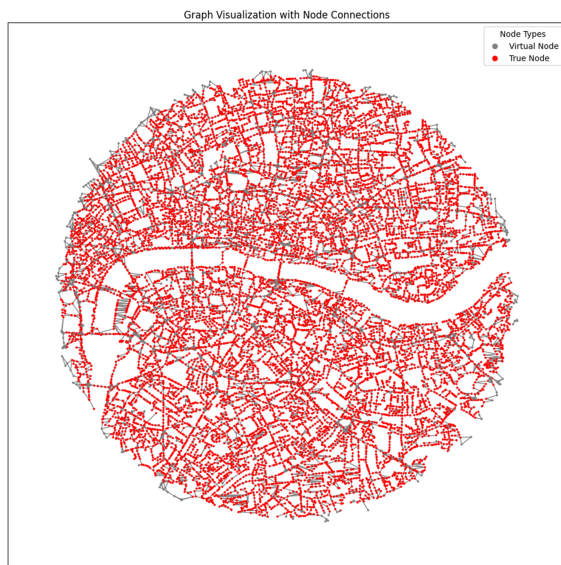


Figure A.12: Right: Steps for connecting SVI locations into a graph based on spatial proximity and road network connections. Virtual nodes are defined to maintain network connection when SVI data is not available on a road segment. Right: A sample graph built based on the logic in London, centring on The Shard.

Appendix B. Landmark Visibility Validation Dataset

Table B.4: Components of validation set for case study 1. For each landmark, the validation set is created by randomly sampling 100 SVIs from distance bands of 0-500 m, 500-1000 m, 1000-1500 m and 1500 m+. The images are then manually labelled as 'visible' and 'invisible' for the corresponding landmark, using Label Studio (Tkachenko et al., 2020).

Tower	Landmark Visible	Landmark Invisible	Total Images
Eiffel Tower	86	314	400
Tokyo Tower	39	361	400
Petronas Towers	97	303	400
The Shard	73	327	400
Taipei 101	103	297	400
Burj Khalifa	195	205	400

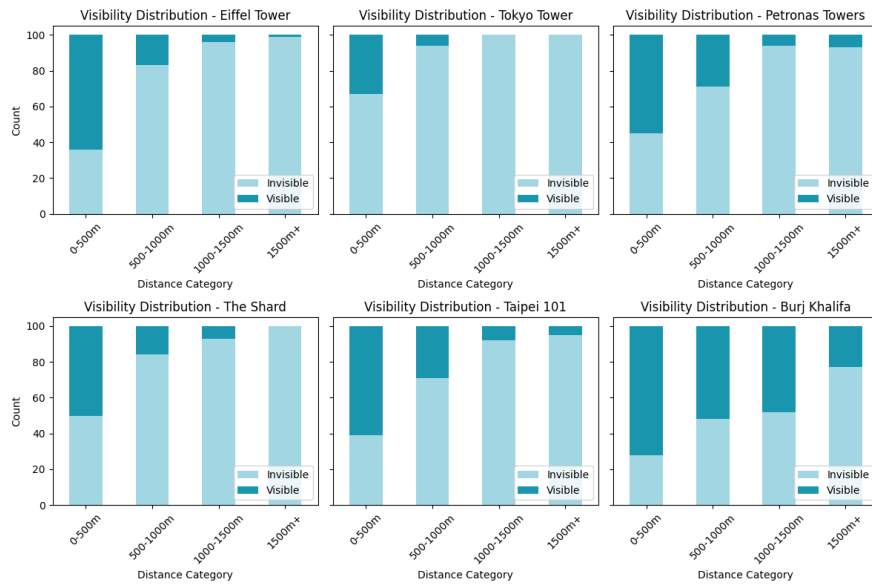


Figure B.13: Distribution of visible and invisible samples within each distance band in the validation set.

Appendix C. Data Sources for 3D visibility Simulations

Table C.5: Data sources for 3D city model generation with VoxCity. "Base" and "Comp." represent base and complementary data for building footprint and height. Complementary data is used to complement missing building height values in the base data.

Landmark	Building Footprint and Height	Tree Canopy Height	Terrain Elevation
The Shard	Base: OSM, Comp.: England 1m Composite DTM/DSM (Environment Agency, 2024b,a)	High Resolution 1m Global Canopy Height Maps (Tolan et al., 2024)	England 1m Composite DTM (Environment Agency, 2024b)
Petronas Towers	Base: OSM, Comp.: Open Building 2.5D Temporal (Sirko et al., 2023)	High Resolution 1m Global Canopy Height Maps (Tolan et al., 2024)	FABDEM (Hawker et al., 2022)
Tokyo Tower	Base: OSM, Comp.: UT-GLOBUS (Kamath et al., 2024)	High Resolution 1m Global Canopy Height Maps (Tolan et al., 2024)	FABDEM
Eiffel Tower	EUBUCCO (Milojevic-Dupont et al., 2023)	High Resolution 1m Global Canopy Height Maps (Tolan et al., 2024)	RGE ALTI (National Institute of Geographic and Forest Information, 2024)
Taipei 101	Base: OSM, Comp.: None	High Resolution 1m Global Canopy Height Maps (Tolan et al., 2024)	FABDEM
Burj Khalifa	Base: OSM, Comp.: None	High Resolution 1m Global Canopy Height Maps (Tolan et al., 2024)	FABDEM

Appendix D. Metrics Comparison between SVI and 3D Methods



Figure D.14: Heatmaps illustrating the precision and recall metrics for SVI-based and 3D-based visibility analysis.

Appendix E. Spatial Distribution of Dice Coefficients

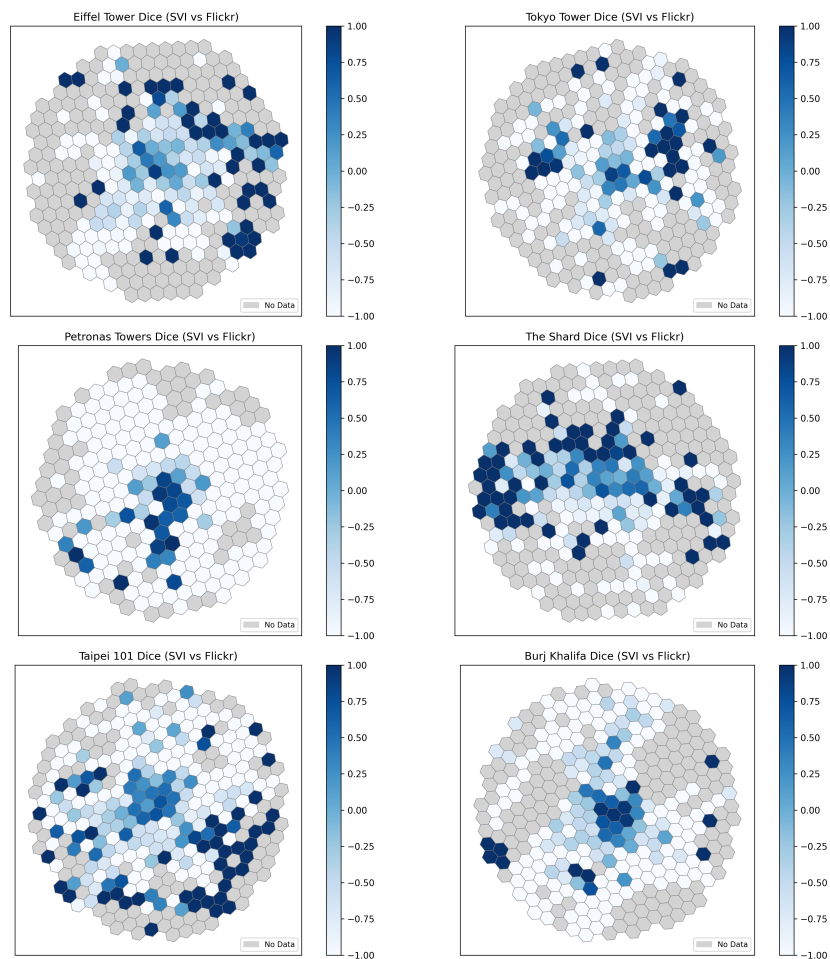


Figure E.15: Spatial distribution of dice coefficients for different landmarks. The larger the dice coefficients, the higher the extent to which the distributions of landmark-visible SVI and Flickr images overlap.

Appendix F. Bridge-Passing Visibility-Accessibility-Visibility (VAV) Paths

Table F.6: VAV paths identified that pass bridges over the River Thames within the case study area. There are a total of 9 bridges with the paths summarised. Among them, the Tower Bridge is the most prominent for supporting the VAV paths, serving as both a landmark and a viewpoint.

Name	Path Count	Percentage
Blackfriars Bridge	35	1.72%
Hungerford Bridge and Golden Jubilee Bridges	21	1.03%
Lambeth Bridge	9	0.44%
London Bridge	136	6.70%
Millennium Bridge	25	1.23%
Southwark Bridge	46	2.26%
Tower Bridge	243	11.96%
Waterloo Bridge	13	0.64%
Westminster Bridge	62	3.05%
Total	590	29.05%

References

- Alphan, H., 2021. Modelling potential visibility of wind turbines: A geospatial approach for planning and impact mitigation. *Renewable and Sustainable Energy Reviews* 152, 111675. URL: <https://www.sciencedirect.com/science/article/pii/S1364032121009497>, doi:10.1016/j.rser.2021.111675.
- Amidon, E.L., Elsner, G.H., 1968. Delineating landscape view areas...a computer approach. Res. Note PSW-RN-180. Berkeley, CA: U.S. Department of Agriculture, Forest Service, Pacific Southwest Forest and Range Experiment Station. 5 p URL: <https://research.fs.usda.gov/treesearch/38437>.
- Anguelov, D., Dulong, C., Filip, D., Frueh, C., Lafon, S., Lyon, R., Ogale, A., Vincent, L., Weaver, J., 2010. Google Street View: Capturing the World at Street Level. *Computer* 43, 32–38. URL: <https://ieeexplore.ieee.org/document/5481932/authors>, doi:10.1109/MC.2010.170.
- Ashrafi, B., Kloos, M., Neugebauer, C., 2021. Heritage Impact Assessment, beyond an Assessment Tool: A comparative analysis of urban development impact on visual integrity in four UNESCO World Heritage Properties. *Journal of Cultural Heritage* 47, 199–207. URL: <https://www.sciencedirect.com/science/article/pii/S1296207420304337>, doi:10.1016/j.culher.2020.08.002.
- Bai, J., Bai, S., Yang, S., Wang, S., Tan, S., Wang, P., Lin, J., Zhou, C., Zhou, J., 2023. Qwen-VL: A Versatile Vision-Language Model for Understanding, Localization, Text Reading, and Beyond. URL: <http://arxiv.org/abs/2308.12966>, doi:10.48550/arXiv.2308.12966. arXiv:2308.12966 [cs].
- Bartie, P., Mackaness, W., Petrenz, P., Dickinson, A., 2015. Identifying related landmark tags in urban scenes using spatial and semantic clustering. *Computers, Environment and Urban Systems* 52, 48–57. URL: <https://www.sciencedirect.com/science/article/pii/S0198971515000381>, doi:10.1016/j.compenvurbsys.2015.03.003.
- Batty, M., 2001. Exploring Isovist Fields: Space and Shape in Architectural and Urban Morphology. *Environment and Planning B: Planning and Design* 28, 123–150. URL: <https://doi.org/10.1068/b2725>, doi:10.1068/b2725.

- Belcher, R.N., Murray, K.A., Reeves, J.P., Fecht, D., 2024. Socioeconomic deprivation modifies green space and mental health associations: A within person study. *Environment International* 192, 109036. URL: <https://www.sciencedirect.com/science/article/pii/S0160412024006226>, doi:10.1016/j.envint.2024.109036.
- Benedikt, M.L., 1979. To Take Hold of Space: Isovists and Isovist Fields. *Environment and Planning B: Planning and Design* 6, 47–65. URL: <https://journals.sagepub.com/action/showAbstract>, doi:10.1068/b060047.
- Bruns, C.R., Chamberlain, B.C., 2019. The influence of landmarks and urban form on cognitive maps using virtual reality. *Landscape and Urban Planning* 189, 296–306. URL: <https://www.sciencedirect.com/science/article/pii/S0169204618303104>, doi:10.1016/j.landurbplan.2019.05.006.
- Cilliers, D., Cloete, M., Bond, A., Retief, F., Alberts, R., Roos, C., 2023. A critical evaluation of visibility analysis approaches for visual impact assessment (VIA) in the context of environmental impact assessment (EIA). *Environmental Impact Assessment Review* 98, 106962. URL: <https://www.sciencedirect.com/science/article/pii/S0195925522002281>, doi:10.1016/j.eiar.2022.106962.
- City of Vancouver, 2024. Public views. URL: <https://vancouver.ca/home-property-development/protecting-public-views.aspx>.
- Cuckovic, Z., 2016. Advanced viewshed analysis: a Quantum GIS plug-in for the analysis of visual landscapes. *Journal of Open Source Software* 1, 32. URL: <https://joss.theoj.org/papers/10.21105/joss.00032>, doi:10.21105/joss.00032.
- Czyńska, K., Rubinowicz, P., 2019. Classification of cityscape areas according to landmarks visibility analysis. *Environmental Impact Assessment Review* 76, 47–60. URL: <https://www.sciencedirect.com/science/article/pii/S0195925518302348>, doi:10.1016/j.eiar.2019.01.004.
- Déderix, S., 2019. Patterns of Visibility, Intervisibility and Invisibility at Bronze Age Apesokari (Crete). *Open Archaeology* 5, 187–203. URL: <https://www.degruyterbrill.com/document/doi/10.1515/opar-2019-0014/html>, doi:10.1515/opar-2019-0014.

- Environment Agency, 2024a. Lidar composite digital surface model (dsm) - 1m. URL: <https://environment.data.gov.uk/dataset/9ba4d5ac-d596-445a-9056-dae3ddec0178>. accessed: 2024-11-13.
- Environment Agency, 2024b. Lidar composite digital terrain model (dtm) - 1m. URL: <https://environment.data.gov.uk/dataset/13787b9a-26a4-4775-8523-806d13af58fc>. accessed: 2024-11-13.
- Epstein, R.A., Patai, E.Z., Julian, J.B., Spiers, H.J., 2017. The cognitive map in humans: spatial navigation and beyond. *Nature Neuroscience* 20, 1504–1513. URL: <https://www.nature.com/articles/nn.4656>, doi:10.1038/nn.4656.
- ESRI, 2021. Visibility (Spatial Analyst)—ArcMap | Documentation. URL: <https://desktop.arcgis.com/en/arcmap/latest/tools/spatial-analyst-toolbox/visibility.htm>.
- Evans, G.W., , Catherine, S., , Pezdek, K., 1982. Cognitive Maps and Urban Form. *Journal of the American Planning Association* 48, 232–244. URL: <https://doi.org/10.1080/01944368208976543>, doi:10.1080/01944368208976543. _eprint: <https://doi.org/10.1080/01944368208976543>.
- Fan, Z., Feng, C.C., Biljecki, F., 2025. Coverage and bias of street view imagery in mapping the urban environment. *Computers, Environment and Urban Systems* 117, 102253. URL: <https://www.sciencedirect.com/science/article/pii/S0198971525000067>, doi:10.1016/j.compenvurbsys.2025.102253.
- Filomena, G., Verstegen, J.A., 2021. Modelling the effect of landmarks on pedestrian dynamics in urban environments. *Computers, Environment and Urban Systems* 86, 101573. URL: <https://www.sciencedirect.com/science/article/pii/S0198971520303069>, doi:10.1016/j.compenvurbsys.2020.101573.
- Fisher-Gewirtzman, D., Shashkov, A., Doytsher, Y., 2013. Voxel based volumetric visibility analysis of urban environments. *Survey Review* 45, 451–461. URL: <https://doi.org/10.1179/1752270613Y.0000000059>, doi:10.1179/1752270613Y.0000000059. _eprint: <https://doi.org/10.1179/1752270613Y.0000000059>.

- Foltête, J.C., Ingensand, J., Blanc, N., 2020. Coupling crowd-sourced imagery and visibility modelling to identify landscape preferences at the panorama level. *Landscape and Urban Planning* 197, 103756. URL: <https://www.sciencedirect.com/science/article/pii/S0169204619313805>, doi:10.1016/j.landurbplan.2020.103756.
- Franco, S.F., Macdonald, J.L., 2018. The effects of cultural heritage on residential property values: Evidence from Lisbon, Portugal. *Regional Science and Urban Economics* 70, 35–56. URL: <https://www.sciencedirect.com/science/article/pii/S0166046218300358>, doi:10.1016/j.regsciurbeco.2018.02.001.
- Fujiwara, K., Ito, K., Ignatius, M., Biljecki, F., 2024. A panorama-based technique to estimate sky view factor and solar irradiance considering transmittance of tree canopies. *Build. Environ.* 266, 112071.
- Fujiwara, K., Tsurumi, R., Kiyono, T., Fan, Z., Liang, X., Lei, B., Yap, W., Ito, K., Biljecki, F., 2026. VoxCity: A seamless framework for open geospatial data integration, grid-based semantic 3D city model generation, and urban environment simulation. *Computers, Environment and Urban Systems* 123, 102366. URL: <https://www.sciencedirect.com/science/article/pii/S019897152500119X>, doi:10.1016/j.compenurbsys.2025.102366.
- Gillings, M., Wheatley, D., 2001. Seeing is not believing: unresolved issues in archaeological visibility analysis, Office for Official Publications of the European Communities, pp. 25–36. URL: <https://eprints.soton.ac.uk/28803/>. conference Name: Proceedings of the COST G2 Working Group 2 round table (18/12/98 - 22/12/98) Meeting Name: Proceedings of the COST G2 Working Group 2 round table (18/12/98 - 22/12/98).
- Greater London Authority, 2012. London View Management Framework. URL: <https://www.london.gov.uk/programmes-strategies/planning/implementing-london-plan/london-plan-guidance-and-spgs/london-view-management>.
- Hagberg, A.A., Schult, D.A., Swart, P.J., 2008. Exploring Network Structure, Dynamics, and Function using NetworkX, in: Varoquaux, G., Vaught, T., Millman, J. (Eds.), Proceedings of the 7th Python in Science Conference, Pasadena, CA USA. pp. 11 – 15.

- Hawker, L., Uhe, P., Paulo, L., Sosa, J., Savage, J., Sampson, C., Neal, J., 2022. A 30m global map of elevation with forests and buildings removed. *Environ. Res. Lett.* 17, 024016.
- Hillier, B., 1996. *Space is the machine: a configurational theory of architecture* / Bill Hillier. Cambridge University Press, New York ; Cambridge. URL: <http://eprints.ucl.ac.uk/archive/00003881/01/SITM.pdf>.
- Hillier, B., Hanson, J., 1984. *The Social Logic of Space*. Cambridge University Press, Cambridge. URL: <https://www.cambridge.org/core/books/social-logic-of-space/6B0A078C79A74FOCC615ACD8B250A985>, doi:10.1017/CB09780511597237.
- Hosseini Alamdari, A., Daneshjoo, K., Yeganeh, M., 2022. New algorithms for generating isovist field and isovist measurements. *Environment and Planning B* 49, 2331–2344. URL: <https://doi.org/10.1177/23998083221083680>, doi:10.1177/23998083221083680.
- Hou, Y., Biljecki, F., 2022. A comprehensive framework for evaluating the quality of street view imagery. *International Journal of Applied Earth Observation and Geoinformation* 115, 103094. URL: <https://www.sciencedirect.com/science/article/pii/S1569843222002825>, doi:10.1016/j.jag.2022.103094.
- Hu, C.B., Zhang, F., Gong, F.Y., Ratti, C., Li, X., 2020. Classification and mapping of urban canyon geometry using Google Street View images and deep multitask learning. *Building and Environment* 167, 106424. URL: <https://www.sciencedirect.com/science/article/pii/S0360132319306341>, doi:10.1016/j.buildenv.2019.106424.
- Huang, W., , Jing, W., , Cong, G., 2024. Zero-shot urban function inference with street view images through prompting a pretrained vision-language model. *International Journal of Geographical Information Science* 38, 1414–1442. URL: <https://doi.org/10.1080/13658816.2024.2347322>, doi:10.1080/13658816.2024.2347322. eprint: <https://doi.org/10.1080/13658816.2024.2347322>.
- Inglis, N.C., Vukomanovic, J., Costanza, J., Singh, K.K., 2022. From viewsheds to viewscapes: Trends in landscape visibility and visual quality research. *Landscape and Urban Planning* 224, 104424. URL: <https://>

www.sciencedirect.com/science/article/pii/S0169204622000731,
doi:10.1016/j.landurbplan.2022.104424.

- Ito, K., Kang, Y., Zhang, Y., Zhang, F., Biljecki, F., 2024. Understanding urban perception with visual data: A systematic review. *Cities* 152, 105169. URL: <https://www.sciencedirect.com/science/article/pii/S0264275124003834>, doi:10.1016/j.cities.2024.105169.
- Ito, K., Zhu, Y., Abdelrahman, M., Liang, X., Fan, Z., Hou, Y., Zhao, T., Ma, R., Fujiwara, K., Ouyang, J., Quintana, M., Biljecki, F., 2025. ZenSVI: An open-source software for the integrated acquisition, processing and analysis of street view imagery towards scalable urban science. *Computers, Environment and Urban Systems* 119, 102283. URL: <https://www.sciencedirect.com/science/article/pii/S0198971525000365>, doi:10.1016/j.compenurbsys.2025.102283.
- Kamath, H.G., Singh, M., Malviya, N., Martilli, A., He, L., Aliaga, D., He, C., Chen, F., Magruder, L.A., Yang, Z.L., Niyogi, D., 2024. GLOBal building heights for urban studies (UT-GLOBUS) for city- and street- scale urban simulations: Development and first applications. *Sci. Data* 11, 886.
- Kim, G., Kim, A., Kim, Y., 2019. A new 3D space syntax metric based on 3D isovist capture in urban space using remote sensing technology. *Computers, Environment and Urban Systems* 74, 74–87. URL: <https://www.sciencedirect.com/science/article/pii/S0198971518301881>, doi:10.1016/j.compenurbsys.2018.11.009.
- Klemmer, K., Rolf, E., Robinson, C., Mackey, L., Rußwurm, M., 2024. SatCLIP: Global, General-Purpose Location Embeddings with Satellite Imagery. URL: <http://arxiv.org/abs/2311.17179>, doi:10.48550/arXiv.2311.17179. arXiv:2311.17179 [cs].
- Klouček, T., Lagner, O., Šímová, P., 2015. How does data accuracy influence the reliability of digital viewshed models? A case study with wind turbines. *Applied Geography* 64, 46–54. URL: <https://www.sciencedirect.com/science/article/pii/S0143622815002131>, doi:10.1016/j.apgeog.2015.09.005.
- Krukar, J., Manivannan, C., Bhatt, M., Schultz, C., 2021. Embodied 3D isovists: A method to model the visual perception of space. *Environment and Planning*

- B: *Urban Analytics and City Science* 48, 2307–2325. URL: <https://doi.org/10.1177/2399808320974533>, doi:10.1177/2399808320974533.
- Landry, N.W., Lucas, M., Iacopini, I., Petri, G., Schwarze, A., Patania, A., Torres, L., 2023. XGI: A Python package for higher-order interaction networks. *Journal of Open Source Software* 8, 5162. URL: <https://doi.org/10.21105/joss.05162>, doi:10.21105/joss.05162.
- Lee, P.U., Tversky, B., 2005. Interplay Between Visual and Spatial: The Effect of Landmark Descriptions on Comprehension of Route/Survey Spatial Descriptions. *Spatial Cognition & Computation* 5, 163–185. URL: <https://doi.org/10.1080/13875868.2005.9683802>, doi:10.1080/13875868.2005.9683802. eprint: <https://doi.org/10.1080/13875868.2005.9683802>.
- Lei, B., , Rudi, S., , Biljecki, F., 2023. Assessing and benchmarking 3D city models. *International Journal of Geographical Information Science* 37, 788–809. URL: <https://doi.org/10.1080/13658816.2022.2140808>, doi:10.1080/13658816.2022.2140808. eprint: <https://doi.org/10.1080/13658816.2022.2140808>.
- Li, S., Liu, P., Stouffs, R., 2025. Fine-grained local climate zone classification using graph networks: A building-centric approach. *Building and Environment* 278, 112928. URL: <https://www.sciencedirect.com/science/article/pii/S036013232500410X>, doi:10.1016/j.buildenv.2025.112928.
- Liu, S., Zeng, Z., Ren, T., Li, F., Zhang, H., Yang, J., Jiang, Q., Li, C., Yang, J., Su, H., Zhu, J., Zhang, L., 2024. Grounding DINO: Marrying DINO with Grounded Pre-Training for Open-Set Object Detection. URL: <http://arxiv.org/abs/2303.05499>, doi:10.48550/arXiv.2303.05499. arXiv:2303.05499 [cs].
- Lopes, A.S., Macedo, D.V., Brito, A.Y.S., Furtado, V., 2019. Assessment of urban cultural-heritage protection zones using a co-visibility-analysis tool. *Computers, Environment and Urban Systems* 76, 139–149. URL: <https://www.sciencedirect.com/science/article/pii/S0198971519300493>, doi:10.1016/j.compenvurbsys.2019.04.009.
- Lu, Y., Gou, Z., Ye, Y., Sheng, Q., 2019. Three-dimensional visibility graph analysis and its application. *Environment and Planning B* 46, 948–962. URL: <https://doi.org/10.1177/2399808317739893>, doi:10.1177/2399808317739893.

- Lynch, K., 1996. *The image of the city*. The MIT Press, Massachusetts Institute of Technology, Cambridge, Massachusetts ; London, England.
- Manahasa, E., , Manahasa, O., 2024. The role of landmarks in shaping Tirana's urban identity: the shift from socialist to post-socialist city. *European Planning Studies* 32, 1029–1058. URL: <https://doi.org/10.1080/09654313.2023.2249508>, doi:10.1080/09654313.2023.2249508. eprint: <https://doi.org/10.1080/09654313.2023.2249508>.
- Middel, A., Lukasczyk, J., Maciejewski, R., Demuzere, M., Roth, M., 2018. Sky View Factor footprints for urban climate modeling. *Urban Climate* 25, 120–134. URL: <https://www.sciencedirect.com/science/article/pii/S2212095518301883>, doi:10.1016/j.uclim.2018.05.004.
- Milojevic-Dupont, N., Wagner, F., Nachtigall, F., Hu, J., Brüser, G.B., Zumwald, M., Biljecki, F., Heeren, N., Kaack, L.H., Pichler, P.P., Creutzig, F., 2023. EU-BUCCO v0.1: European building stock characteristics in a common and open database for 200+ million individual buildings. *Sci Data* 10, 147.
- Minderer, M., Gritsenko, A., Houlsby, N., 2024. Scaling Open-Vocabulary Object Detection. URL: <http://arxiv.org/abs/2306.09683>, doi:10.48550/arXiv.2306.09683. arXiv:2306.09683 [cs] version: 3.
- Minderer, M., Gritsenko, A., Stone, A., Neumann, M., Weissenborn, D., Dosovitskiy, A., Mahendran, A., Arnab, A., Dehghani, M., Shen, Z., Wang, X., Zhai, X., Kipf, T., Houlsby, N., 2022. Simple Open-Vocabulary Object Detection with Vision Transformers. URL: <http://arxiv.org/abs/2205.06230>, doi:10.48550/arXiv.2205.06230. arXiv:2205.06230 [cs].
- Mor, M., Fisher-Gewirtzman, D., Yosifof, R., Dalyot, S., 2021. 3D Visibility Analysis for Evaluating the Attractiveness of Tourism Routes Computed from Social Media Photos. *ISPRS International Journal of Geo-Information* 10, 275. URL: <https://www.mdpi.com/2220-9964/10/5/275>, doi:10.3390/ijgi10050275. number: 5.
- Morello, E., Ratti, C., 2009. A Digital Image of the City: 3D Isovists in Lynch's Urban Analysis. *Environment and Planning B: Planning and Design* 36, 837–853. URL: <https://journals.sagepub.com/action/showAbstract>, doi:10.1068/b34144t.

- Natapov, A., Czamanski, D., Fisher-Gewirtzman, D., 2013. Can visibility predict location? Visibility graph of food and drink facilities in the city. *Survey Review* 45, 462–471. URL: <https://doi.org/10.1179/1752270613Y.0000000057>, doi:10.1179/1752270613Y.0000000057. _eprint: <https://doi.org/10.1179/1752270613Y.0000000057>.
- National Institute of Geographic and Forest Information, 2024. Rge alti® 1m. URL: <https://geoservices.ign.fr/rgealti>. accessed: 2024-11-13.
- Neteler, M., Bowman, M.H., Landa, M., Metz, M., 2012. GRASS GIS: A multi-purpose open source GIS. *Environmental Modelling & Software* 31, 124–130. URL: <https://linkinghub.elsevier.com/retrieve/pii/S1364815211002775>, doi:10.1016/j.envsoft.2011.11.014.
- Omer, I., Goldblatt, R., 2007. The implications of inter-visibility between landmarks on wayfinding performance: An investigation using a virtual urban environment. *Computers, Environment and Urban Systems* 31, 520–534. URL: <https://www.sciencedirect.com/science/article/pii/S0198971507000555>, doi:10.1016/j.compenvurbsys.2007.08.004.
- Omrani Azizabad, S., Mahdavinejad, M., Hadighi, M., 2024. Three-dimensional embodied visibility graph analysis: Investigating and analyzing values along an outdoor path. *Environment and Planning B* , 23998083241303199 URL: <https://doi.org/10.1177/23998083241303199>, doi:10.1177/23998083241303199.
- OpenAI, 2022. CLIP: Connecting text and images. URL: <https://openai.com/index/clip/>.
- OpenAI, 2024. Hello GPT-4o. URL: <https://openai.com/index/hello-gpt-4o/>.
- Pearson, K., 1905. The Problem of the Random Walk. *Nature* 72, 294–294. URL: <https://www.nature.com/articles/072294b0>, doi:10.1038/072294b0.
- Pyka, K., Piskorski, R., Jasińska, A., 2022. LiDAR-based method for analysing landmark visibility to pedestrians in cities: case study in Kraków, Poland. *International Journal of Geographical Information Science* 36, 476–495. URL: <https://doi.org/10.1080/13658816.2021.2015600>, doi:10.1080/13658816.2021.2015600. _eprint: <https://doi.org/10.1080/13658816.2021.2015600>.

- Radford, A., Kim, J.W., Hallacy, C., Ramesh, A., Goh, G., Agarwal, S., Sastry, G., Aspell, A., Mishkin, P., Clark, J., Krueger, G., Sutskever, I., 2021. Learning Transferable Visual Models From Natural Language Supervision. URL: <http://arxiv.org/abs/2103.00020>, doi:10.48550/arXiv.2103.00020. arXiv:2103.00020 [cs].
- Ratti, C., 2004. Space Syntax: Some Inconsistencies. *Environment and Planning B: Planning and Design* 31, 487–499. URL: <https://doi.org/10.1068/b3019>, doi:10.1068/b3019.
- Santosa, H., Yudono, A., Sutikno, F.R., Adhitama, M.S., Tolle, H., Zuliana, E., 2023. Visibility Evaluation of Historical Landmark Building Using Photographic Survey Coupled with Isovist and Viewshed Analysis. *International Review for Spatial Planning and Sustainable Development* 11, 71–92. doi:10.14246/irspsd.11.4_71.
- Shen, Y., Wu, Z., 2022. Functional visibility graph analysis: Quantifying visuo-functional space with social media check-in data. *Environment and Planning B: Urban Analytics and City Science* 49, 41–57. URL: <https://doi.org/10.1177/23998083211001840>, doi:10.1177/23998083211001840.
- Sirko, W., Bremping, E.A., Marcos, J.T.C., Annkah, A., Korme, A., Hassen, M.A., Sapkota, K., Shekel, T., Diack, A., Nevo, S., Hickey, J., Quinn, J., 2023. High-resolution building and road detection from sentinel-2. arXiv [cs.CV] .
- Snopková, D., De Cock, L., Juřík, V., Kvarda, O., Tancoš, M., Herman, L., Kubíček, P., 2023. Isovists compactness and stairs as predictors of evacuation route choice. *Scientific Reports* 13, 2970. URL: <https://www.nature.com/articles/s41598-023-29944-8>, doi:10.1038/s41598-023-29944-8.
- Swietek, A.R., Zumwald, M., 2023. Visual Capital: Evaluating building-level visual landscape quality at scale. *Landscape and Urban Planning* 240, 104880. URL: <https://www.sciencedirect.com/science/article/pii/S0169204623001998>, doi:10.1016/j.landurbplan.2023.104880.
- Talamini, G., Liu, T., El-Khoury, R., Shao, D., 2023. Visibility and symbolism of corporate architecture: A multi-method approach for visual impact assessment. *Environment and Planning B* 50, 2407–2429. URL: <https://doi.org/10.1177/23998083231154587>, doi:10.1177/23998083231154587.

- Tandy, C., 1967. The isovist method of landscape survey. *Methods of landscape analysis* , 9–10.
- Tavernor, R., 2007. Visual and cultural sustainability: The impact of tall buildings on London. *Landscape and Urban Planning* 83, 2–12. URL: <https://www.sciencedirect.com/science/article/pii/S0169204607001399>, doi:10.1016/j.landurbplan.2007.05.010.
- Tkachenko, M., Malyuk, M., Holmanyuk, A., Liubimov, N., 2020. Label Studio: Data labeling software. URL: <https://github.com/HumanSignal/label-studio>.
- Tolan, J., Yang, H.I., Nosarzewski, B., Couairon, G., Vo, H.V., Brandt, J., Spore, J., Majumdar, S., Haziza, D., Vamaraju, J., Moutakanni, T., Bojanowski, P., Johns, T., White, B., Tiede, T., Couprie, C., 2024. Very high resolution canopy height maps from RGB imagery using self-supervised vision transformer and convolutional decoder trained on aerial lidar. *Remote Sens. Environ.* 300, 113888.
- Truchet, S., Piguet, V., Aubert, F., Callois, J.M., 2016. Spatial influence of attractions on tourism development. *Tourism Geographies* 18, 539–560. URL: <https://doi.org/10.1080/14616688.2016.1221985>, doi:10.1080/14616688.2016.1221985. eprint: <https://doi.org/10.1080/14616688.2016.1221985>.
- Turan, I., Chegut, A., Fink, D., Reinhart, C., 2021. Development of view potential metrics and the financial impact of views on office rents. *Landscape and Urban Planning* 215, 104193. URL: <https://www.sciencedirect.com/science/article/pii/S0169204621001560>, doi:10.1016/j.landurbplan.2021.104193.
- Turner, A., Doxa, M., O’Sullivan, D., Penn, A., 2001. From Isovists to Visibility Graphs: A Methodology for the Analysis of Architectural Space. *Environment and Planning B: Planning and Design* 28, 103–121. URL: <https://journals.sagepub.com/doi/10.1068/b2684>, doi:10.1068/b2684.
- Varoudis, T., Psarra, S., 2014. Beyond two dimensions: architecture through three dimensional visibility graph analysis. *The Journal of Space Syntax* 5, 91–108. URL: <http://joss.bartlett.ucl.ac.uk/journal/index.php/joss/article/view/200>. number: 1.

- Wang, M., Zheng, D., Ye, Z., Gan, Q., Li, M., Song, X., Zhou, J., Ma, C., Yu, L., Gai, Y., Xiao, T., He, T., Karypis, G., Li, J., Zhang, Z., 2020. Deep Graph Library: A Graph-Centric, Highly-Performant Package for Graph Neural Networks. URL: <http://arxiv.org/abs/1909.01315>, doi:10.48550/arXiv.1909.01315. arXiv:1909.01315 [cs].
- Wang, W., Lv, Q., Yu, W., Hong, W., Qi, J., Wang, Y., Ji, J., Yang, Z., Zhao, L., Song, X., Xu, J., Xu, B., Li, J., Dong, Y., Ding, M., Tang, J., 2024. CogVLM: Visual Expert for Pretrained Language Models. URL: <http://arxiv.org/abs/2311.03079>, doi:10.48550/arXiv.2311.03079. arXiv:2311.03079 [cs].
- Wiener, J.M., Franz, G., 2005. Isovists as a Means to Predict Spatial Experience and Behavior, in: Freksa, C., Knauff, M., Krieg-Brückner, B., Nebel, B., Barkowsky, T. (Eds.), Spatial Cognition IV. Reasoning, Action, Interaction, Springer, Berlin, Heidelberg. pp. 42–57. doi:10.1007/978-3-540-32255-9_3.
- Wood, S.A., Guerry, A.D., Silver, J.M., Lacayo, M., 2013. Using social media to quantify nature-based tourism and recreation. *Scientific Reports* 3, 2976. URL: <https://www.nature.com/articles/srep02976>, doi:10.1038/srep02976.
- Wróżyński, R., Pyszny, K., Wróżyńska, M., 2024. Reaching beyond GIS for comprehensive 3D visibility analysis. *Landscape and Urban Planning* 247, 105074. URL: <https://www.sciencedirect.com/science/article/pii/S0169204624000732>, doi:10.1016/j.landurbplan.2024.105074.
- Wu, B., Yu, B., Shu, S., Liang, H., Zhao, Y., Wu, J., 2021. Mapping fine-scale visual quality distribution inside urban streets using mobile LiDAR data. *Building and Environment* 206, 108323. URL: <https://www.sciencedirect.com/science/article/pii/S0360132321007216>, doi:10.1016/j.buildenv.2021.108323.
- Xia, F., Liu, J., Nie, H., Fu, Y., Wan, L., Kong, X., 2020. Random Walks: A Review of Algorithms and Applications. *IEEE Transactions on Emerging Topics in Computational Intelligence* 4, 95–107. URL: <https://ieeexplore.ieee.org/abstract/document/8911513>, doi:10.1109/TETCI.2019.2952908.

- Xu, Y., Chen, R., Du, H., Chen, M., Fu, C., Li, Y., 2025. Evaluation of green space influence on housing prices using machine learning and urban visual intelligence. *Cities* 158, 105661. URL: <https://www.sciencedirect.com/science/article/pii/S0264275124008758>, doi:10.1016/j.cities.2024.105661.
- Yang, J., Rong, H., Kang, Y., Zhang, F., Chegut, A., 2021. The financial impact of street-level greenery on New York commercial buildings. *Landscape and Urban Planning* 214, 104162. URL: <https://www.sciencedirect.com/science/article/pii/S0169204621001250>, doi:10.1016/j.landurbplan.2021.104162.
- Yap, W., Stouffs, R., Biljecki, F., 2023. Urbanity: automated modelling and analysis of multidimensional networks in cities. *npj Urban Sustainability* 3, 1–11. URL: <https://www.nature.com/articles/s42949-023-00125-w>, doi:10.1038/s42949-023-00125-w.
- Yesiltepe, D., Conroy Dalton, R., Ozbil Torun, A., 2021. Landmarks in wayfinding: a review of the existing literature. *Cognitive Processing* 22, 369–410. URL: <https://doi.org/10.1007/s10339-021-01012-x>, doi:10.1007/s10339-021-01012-x.
- Zhao, Y., Wu, B., Wu, J., Shu, S., Liang, H., Liu, M., Badenko, V., Fedotov, A., Yao, S., Yu, B., 2020. Mapping 3D visibility in an urban street environment from mobile LiDAR point clouds. *GIScience & Remote Sensing* 57, 797–812. URL: <https://doi.org/10.1080/15481603.2020.1804248>, doi:10.1080/15481603.2020.1804248. eprint: <https://doi.org/10.1080/15481603.2020.1804248>.